JACS
JOURNAL OF THE AMERICAN CHEMICAL SOCIETY

ARTICLE

pubs.acs.org/JACS

Synthesis and Stability of Homoleptic Metal(III) Tetramethylaluminates

Giovanni Occhipinti,[†] Christian Meermann,[†] H. Martin Dietrich,[†] Rannveig Litlabø,[†] Florian Auras,[‡] Karl W. Törnroos,[†] Cäcilia Maichle-Mössmer,[§] Vidar R. Jensen,[†,*] and Reiner Anwander[†,§,*]

[†]Department of Chemistry, University of Bergen, Allégaten 41, N-5007 Bergen, Norway

[‡]Institut für Physik, Universität Augsburg, Universitätsstrasse 1, D-86159 Augsburg, Germany

[§]Institut für Anorganische Chemie, Universität Tübingen, Auf der Morgenstelle 18, D-72076 Tübingen, Germany

Supporting Information

ABSTRACT: Whereas a number of homoleptic metal(III) tetramethylaluminates $M(AlMe_4)_3$ of the rare earth metals have proven accessible, the stability of these compounds varies strongly among the metals, with some even escaping preparation altogether. The differences in stability may seem puzzling given that this class of metals usually is considered to be relatively uniform with respect to properties. On the basis of quantum chemically obtained relative energies and atomic and molecular descriptors of homoleptic tris(tetramethylaluminate) and related compounds of rare earth metals, transition metals, p-block metals, and actinides, multivariate modeling has identified the importance of ionic metal−methylaluminate bonding and small steric repulsion between the methylaluminate ligands for obtaining stable homoleptic compounds. Low electronegativity and a sufficiently large ionic radius are thus essential properties for the central metal atom. Whereas scandium and many transition metals are too small and too electronegative for this task, all lanthanides and actinides covered in this study are predicted to give homoleptic compounds stable toward loss of trimethylaluminum, the expected main decomposition reaction. Three of the predicted lanthanide-based compounds $Ln(AlMe_4)_3$ (Ln = Ce, Tm, Yb) have been prepared and fully characterized in the present work, in addition to $Ln(OCH_2tBu)_3(AlMe_3)_3$ (Ln = Sc, Nd) and $[Eu(AlEt_4)_2]_n$. At ambient temperature, donor-free hexane solutions of $Ln(AlMe_4)_3$ of the Ln^{3+}/Ln^{2+} redox-active metal centers display enhanced reduction to $[Ln(AlMe_4)_2]_n$ with decreasing negative redox potential, in the order Eu ≫ Yb ≫ Sm. Whereas $Eu(AlMe_4)_3$ could not be identified, $Yb(AlMe_4)_3$ turned out to be isolable in low yield. All attempts to prepare the putative $Sc(AlMe_4)_3$, featuring the smallest rare earth metal center, failed.

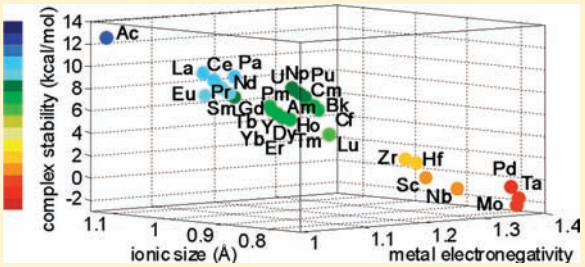

INTRODUCTION

Transition-metal-bonded tetraalkylaluminate moieties have been identified as fundamental intermediates in Ziegler−Natta-type polymerization catalysis crucially affecting the formation of dormant species (resting states), chain transfer reactions, and the reduction of the transition metal center (e.g., $Ti^{4+} \rightarrow Ti^{3+}$).[1] As a result of their transient nature and proneness to (multiple) C−H bond activation,[2] such transition-metal-based tetraalkylaluminate complexes escaped X-ray structural characterizations[3,4] except for the cationic heteroleptic Ti^{4+} compound $[Ti(NtBu)(Me_3[9]aneN_3)(\mu\text{-}Me)_2AlMe_2][B(C_6F_5)_4]$.[5] In contrast, there is a plethora of thermally stable tetraalkylaluminate complexes of the alkali,[6,7] alkaline earth,[8] and rare earth metals (Ln).[9−11] While NMR spectroscopic studies demonstrate the high mobility of the tetraalkylaluminate ligands in solution,[12] the solid-state structures uniquely reveal their capability to cope with the highly ionic bonding by adopting sterically controlled η^n (n = 0, 1, 2, 3) and $\mu-\eta^m{:}\eta^n$ (m = 1; n = 1, 2, 3) coordination modes.[13−19] The trivalent Ln derivatives not only were found as pivotal components in Ziegler catalysts[9,20] but also emerged as robust versions of conventional alkyl complexes ("alkyls in disguise") efficiently promoting protonolysis[21] and salt metathesis reactions.[22] Moreover, the enhanced reactivity of Ln^{3+}−AlR_4 moieties facilitates the synthesis of formerly elusive imido,[23] methylene,[24] methine,[25] and even carbide species[26] via organoaluminum-assisted multiple C(N)−H activation.[27]

The parent homoleptic rare earth metal(III) tetramethylaluminates $Ln(AlMe_4)_3$ have been synthesized and fully characterized for differently sized lanthanide metal centers, Ln = Y (X-ray),[10a] La (X-ray),[10d] Ce,[10d] Pr (X-ray),[10d] Nd (X-ray, neutron diffraction),[10a,b] Sm (X-ray),[10d] Ho,[10d] and Lu (X-ray).[10d] The preferred reaction protocol has been an AlR_3-mediated [amide] → [alkyl] transformation. Surprisingly, the synthesis and isolation of the derivative involving the smallest and hence most Lewis acidic Ln^{3+} center, the putative $Sc(AlMe_4)_3$, failed so far,[28] even though it has been possible to isolate heteroleptic tetraalkylaluminate complexes including $(C_5H_5)_2Sc(AlMe_4)$,[29]

Received: January 5, 2011
Published: April 05, 2011

dx.doi.org/10.1021/ja2001049 | J. Am. Chem. Soc. 2011, 133, 6323–6337

Scheme 1. Synthesis Approaches toward Homoleptic Tetramethylaluminates $Ln(AlMe_4)_3$

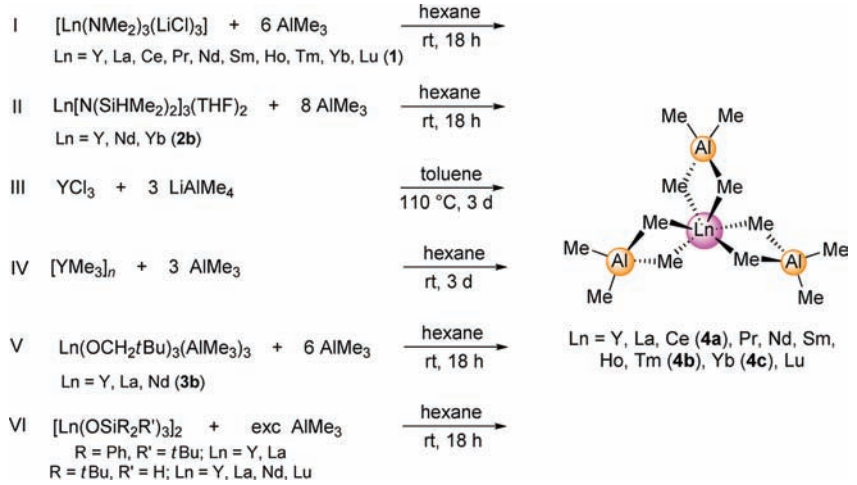

$Sc\{NC_5H_3[CH_2N(C_6H_3iPr_2\text{-}2,6)]_2\text{-}2,6\}(AlMe_4)$,[30] $\{[(C_6H_5CH_2O)_2\text{-}25,27](t\text{Bu-}4)\text{calix}[4]\text{arene}\}Sc(AlMe_4)$,[30] $\{[(CH_3O)_2\text{-}25,27]\text{-}(t\text{Bu-}4)\text{calix}[4]\text{arene}\}Sc(AlMe_4)$,[30] $(C_5Me_4SiMe_3)Sc(AlMe_4)_2$,[31] and $[fc\{NSi(t\text{Bu})Me_2\}_2]Sc(AlMe_4)(AlMe_3)$[32] (fc = 1,1′-ferrocenylene) as thermally stable compounds. Metallocene derivatives $(C_{12}H_3Me_4iPr_2t\text{Bu})Sc(AlMe_4)$,[33] $[Me_2Si(C_5H_3t\text{Bu})_2]Sc(AlMe_4)$,[34] and $[fc\{NSi(t\text{Bu})Me_2\}_2]Sc(AlMe_4)(AlMe_3)$[32] are so far the only X-ray crystallographically authenticated scandium tetramethylaluminate complexes. The failed isolation of a homoleptic scandium alkylaluminate species might be due to a low thermodynamic stability of $Sc(AlMe_4)_3$ compared to successfully isolated homoleptic compounds of the other rare earth metals. In order to test this hypothesis we have adopted a combined approach involving a new synthesis strategy as well as insight and guidance from quantum chemistry.

To this end, a comparative quantum chemical investigation of a broad selection of homoleptic tetramethylaluminates $M(AlMe_4)_3$ has been performed. The metal centers include, in addition to Sc, the entire set of rare earth metals for which homoleptic tetramethylaluminates have been characterized (Y, La, Ce, Pr, Nd, Sm, Ho, and Lu),[10] a selection of representative transition metals (Ti, Zr, Hf, Nb, and Ta), p-block metals (Al, Ga, In, Tl, Bi), and also actinides (Ac, Th, Pa, U, Np, and Pu). Starting from this diverse set of metals, which effectively span the variation space, and using multivariate classification and modeling, we have extracted the factors governing the stability of the homoleptic compounds and also predicted the stability of a series of hitherto unobserved homoleptic tetramethylaluminates.

Next, three of the lanthanide-based compounds $Ln(AlMe_4)_3$ (Ln = Ce, Tm, Yb) predicted to be stable have been prepared in the present work. Their accessibility and characterization are addressed in detail, as are those of $Ln(OCH_2t\text{Bu})_3(AlMe_3)_3$ (Ln = Sc, Nd) and $[Eu(AlEt_4)_2]_n$. Finally, a series of attempts at preparing the putative $Sc(AlMe_4)_3$ are also described.

RESULTS AND DISCUSSION

Elusive or Nonexistent $Sc(AlMe_4)_3$? Various synthesis approaches are viable to access homoleptic tetramethylaluminate complexes $Ln(AlMe_4)_3$ (I–VI, Scheme 1).[9,10,35,36]

Particularly, route I proved to be of value for the straightforward high-yield synthesis of $Ln(AlMe_4)_3$ for the entire Ln^{3+} (La → Lu) size range, avoiding any ate complex formation.[10] Unfortunately, the amide elimination reactions I and II were "unsuccessful" in the scandium case, and formation of putative $Sc(AlMe_4)_3$ was not observed. Addition of an excess of $AlMe_3$ to complexes $[Sc(NMe_2)_3(LiCl)_3]$ (**1a**) and $Sc[N(SiHMe_2)_2]_3(THF)$ gave only yellow oily products, while repeated trituration with hexane caused the formation of a precipitate. Separation from the solution and evaporation of the volatiles gave finally a beige powder (approach I). Elemental analysis suggested the formation of $[ScMe_3]_n$,[36] consistent with $Sc(AlMe_4)_3$ as an intermediate complex, which loses 3 molecules of $AlMe_3$. ^1H NMR spectra in benzene-d_6, however, revealed complicated reaction mixtures and the formation of various alkylated species, which could not further be identified. The slightly beige color of the solid material as well as the yellow benzene-d_6 solution might be indicative of C–H activation processes.[24–26] Moreover, the scandium amide complex $[Sc(NMe_2)_3(LiCl)_3]$ (**1a**) did not give any isolable $AlMe_3$ adduct complexes $[Sc(NMe_2)_3(AlMe_3)_x]$ ($x \leq 3$), in analogy to structurally characterized $[Nd(NMe_2)_3(AlMe_3)_3]$, obtained from $[Nd(NMe_2)_3(LiCl)_3]$ and 3 equiv of $AlMe_3$.[37]

These attempts, however, led to the same side products, $[\{Me_2AlNR_2\}_2]$ (proved by NMR spectroscopy), as observed in all the successful syntheses of homoleptic tetramethylaluminate complexes of rare earth metals, suggesting that the scandium complexes $[Sc(NMe_2)_3(LiCl)_3]$ and $Sc[N(SiHMe_2)_2]_3(THF)$ react with trimethylaluminum in a fashion similar to that of corresponding complexes of other rare earth metals. Recently, Okuda reported on the reaction of $ScCl_3$ with 3 equiv of $LiAlMe_4$ (III, Scheme 1); however, all attempts in noncoordinating solvents such as CH_2Cl_2, toluene, or hexamethyldisiloxane failed to provide the desired product.[31] These findings prompted us to apply synthesis route V, which utilizes $[Ln(OCH_2t\text{Bu})_3]_4$ as a donor solvent- and alkali metal-free precursor.[38]

In the course of our investigations into the structure–reactivity relationships of rare earth metal-promoted 1,3-diene polymerization we recently investigated neopentoxide trimethylaluminum ($AlMe_3$) adduct complexes $Ln(OCH_2t\text{Bu})_3(AlMe_3)_3$ (Ln = La, Nd, Y) as initiator components for isoprene polymerization.[35,39] Our initial reactivity studies indicated that complexes $Ln(OCH_2t\text{Bu})_3(AlMe_3)_3$ are prone to peralkylation in the presence of excess $AlMe_3$ with formation of $Ln(AlMe_4)_3$.[35] The feasibility of neopentoxide trimethylaluminum adduct complexes as precursors

dx.doi.org/10.1021/ja2001049 |J. Am. Chem. Soc. 2011, 133, 6323–6337

raised hope that $Sc(AlMe_4)_3$ might be accessible via this synthesis route. Discrete rare earth metal aryl(alk)oxide trialkylaluminum compounds of type $Ln(OR)_3(AlMe_3)_x$ have been reported before; however, X-ray crystallographic examinations are so far limited to *tert*-butoxide and 2,6-di-isopropylphenoxide derivatives (see Table 1 for structural parameters of heterobimetallic Ln/Al aryl(alk)oxide trialkylaluminum adduct complexes).[39−50] Evans and co-workers initially reported on homoleptic $Y(OtBu)_3(AlMe_3)_3$, which was obtained as one of three products from the reaction of $Y_3(OtBu_3)_7Cl_2(THF)_2$ with $AlMe_3$.[42] Not long after, Biagini et al. described $Ln(OtBu)_3(AlMe_3)_3$ (Ln = Y, Pr, Nd) and $Nd(OMe)_3(AlMe_3)_3$ and their successful application in 1,3-diene polymerization.[40,41]

Scandium neopentoxide $[Sc(OCH_2tBu)_3]_4$[38] was obtained via protonolysis of $Sc[N(SiMe_3)_2]_3$[51] with $HOCH_2tBu$ according to literature procedures.[40] Additionally, $Sc(NMe_2)_3(LiCl)_3$ (**1a**) was used as a more basic and hence more reactive precursor compound (Scheme 2). Targeting the $[Ln(OCH_2tBu)_3]_4 \rightarrow Ln(AlMe_4)_3$ transformation, we thought it helpful to conduct the scandium and (well-functioning) neodymium reactions in parallel. Accordingly, homoleptic $Ln(OCH_2tBu)_3(AlMe_3)_3$ (Ln = Sc, **3a**; Nd, **3b**) were obtained from the reaction of $[Ln(OCH_2tBu)_3]_4$ with a slight excess of $AlMe_3$, in almost quantitative yield (Scheme 2). The strong Lewis acid $AlMe_3$ disrupts the cage-like structure of tetrameric $[Ln(OCH_2tBu)_3]_4$, forming $LnAl_3$ heterobimetallic complexes both for the large neodymium and small scandium metal centers. Such identical reaction and coordination behavior could not be anticipated. For comparison, aryloxide complexes $Ln(OC_6H_3tBu_2\text{-}2,6)_3$ afford either $AlMe_3$ adduct, $La(OC_6H_3tBu_2\text{-}2,6)_3(AlMe_3)$, or tetramethylaluminate complexes, $Y(OC_6H_3tBu_2\text{-}2,6)_2(AlMe_4)$, depending on the metal size.[45] Variable temperature NMR experiments of complexes **3** are consistent with previous studies of the corresponding yttrium and lanthanum congeners[35] showing decoalescence of bridging and terminal methyl groups at low temperature as well as line sharpening at elevated temperatures.

Scheme 2. Synthesis of $[Sc(OCH_2tBu)_3]_4$ via Amine Elimination Reactions and Adduct Formation with $AlMe_3$

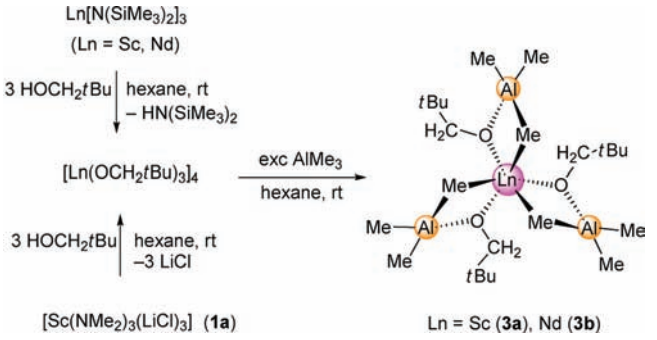

Recrystallization of compounds **3** from saturated hexane solutions at −35 °C gave colorless (**3a**) and light blue single crystals (**3b**) suitable for X-ray structure analyses. Complexes $Ln(OCH_2tBu)_3(AlMe_3)_3$ (Ln = Sc, **3a**; Nd, **3b**), $Nd(OtBu)_3(AlMe_3)_3$,[40] and $Ln[N(SiMe_3)_2]_3$[52] crystallize in the hexagonal space group *P*31*c*. For comparison, aluminate complex $Nd(AlMe_4)_3$ crystallizes in the monoclinic space group $P2_1/n$.[10a] Correspondingly, complexes **3** feature three crystallographically equivalent O,C-chelating $[(\mu\text{-}OCH_2tBu)(\mu\text{-}Me)AlMe_2]$ ligands accomplishing a distorted octahedral coordination geometry (Figure 1, Table 2).[40] In the homoleptic trimethylaluminum adduct **3a** the Sc−$[AlMe_3]$ distances (Sc−C = 2.4784(16) Å, Sc···Al = 3.0297(5) Å)

Table 1. Structural Parameters of Heterobimetallic Ln/Al Aryl(alk)oxide Trialkylaluminum Adduct Complexes

compound	Ln−C (Å)	Ln···Al (Å)	ref
	Alkoxides		
homoleptic			
$Sc(OCH_2tBu)_3(AlMe_3)_3$ (**3a**)	2.4784(16)	3.0297(5)	this work
$Nd(OCH_2tBu)_3(AlMe_3)_3$ (**3b**)	2.6977(15)	3.0297(5)	this work
$Nd(OtBu)_3(AlMe_3)_3$	2.78(1)	3.300	40
$Y(OtBu)_3(AlMe_3)_3$	2.69(3)	3.195(7)	42
$C_{62}H_{154}Al_6Cl_{26}Nd_{12}O_2$	2.585−2.769	2.829	43
heteroleptic			
$Y(OtBu)_3(AlMe_3)_2(THF)$	2.735(6), 2.668(1)	3.244(3), 3.200(3)	42
$(C_5H_4SiMe_3)Y(OtBu)_2(AlMe_3)_2$	2.577(7), 2.562(6)	3.094(2), 3.160(2)	44
$(C_5Me_5)Y(OCH_2tBu)_2(AlMe_3)_2$	2.584(3), 2.576(4)	3.166(1), 3.176(1)	45
$(C_5Me_5)Lu(OCH_2tBu)_2(AlMe_3)_2$	2.540(4), 2.533(4)	3.119(2), 3.123(2)	45
$La(AlMe_4)_2[OSi(OtBu)_3(AlMe_3)]$	2.798(3)/2.668(5)−2.800(4)	3.347(2)/3.310(2), 3.288(2)	46
$Pr(AlMe_4)_2[OSi(OtBu)_3(AlMe_3)]$	2.754(2)/2.618(2)−2.792(2)	3.301(1)/3.263(2), 3.235(2)	10c
	Aryloxides		
homoleptic			
$Y(OC_6H_3iPr_2\text{-}2,6)_3(AlMe_3)_2$	2.544(2), 2.541(2)	3.192(1), 3.187(1)	47
$La(OC_6H_3iPr_2\text{-}2,6)_3(AlMe_3)_2$	2.801(5), 2.759(5)	3.410(3), 3.367(3)	48
$Nd(OC_6H_3iPr_2\text{-}2,6)_3(AlMe_3)_2$	2.652(4), 2.681(6)	3.295(3), 3.312(3)	39
$Sm(OC_6H_3iPr_2\text{-}2,6)_3(AlMe_3)_2$	2.632(5), 2.620(5)	3.284(3), 3.273(3)	49
$Sm(OC_6H_3iPr_2\text{-}2,6)_3(AlEt_3)_2$	2.649(4), 2.627(4)	3.293(2), 3.286(2)	48
heteroleptic			
$Nd[(OC_6H_3Me_2\text{-}2,6)_2AlEt_2](OC_6H_3Me_2\text{-}2,6)_2(THF)_2$		3.411(6)	50
$Y[(OC_6H_3Me_2\text{-}2,6)_2AlMe_2](OC_6H_3Me_2\text{-}2,6)_2(THF)_2$		3.298(7)	50

dx.doi.org/10.1021/ja2001049 |*J. Am. Chem. Soc.* 2011, 133, 6323–6337

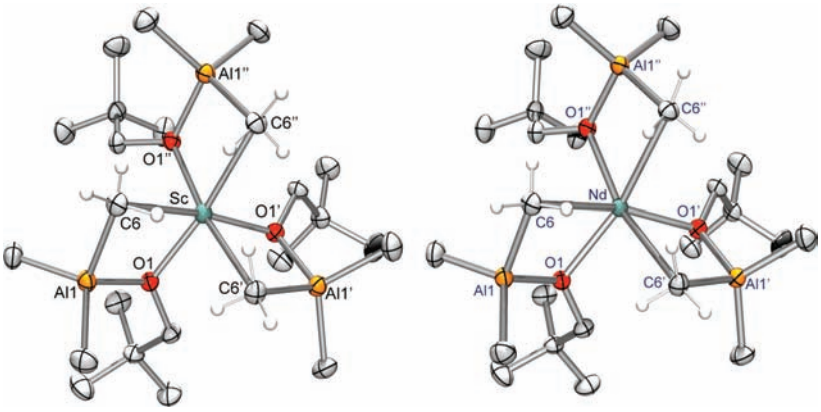

Figure 1. Molecular structures of $Sc(OCH_2tBu)_3(AlMe_3)_3$ (**3a**) and $Nd(OCH_2tBu)_3(AlMe_3)_3$ (**3b**) shown with atomic displacement parameters at the 50% level. The Ln metal atom sits on a crystallographic 3-fold position. Only H-atoms for coordinating methyl groups are indicated.

Table 2. Selected Interatomic Distances and Angles for $Sc(OCH_2tBu)_3(AlMe_3)_3$ (3a) and $Nd(OCH_2tBu)_3(AlMe_3)_3$ (3b)

	3a (Ln = Sc)	**3b** (Ln = Nd)
	Bond Lengths (Å)	
Ln−O1	2.0616(11)	2.2940(10)
Ln−C6	2.4784(16)	2.6977(15)
Ln···Al1	3.0297(5)	3.2756(4)
	Bond Angles (deg)	
O1−Ln−O1	99.30(4)	105.77(3)
C6−Ln−C6	90.82(5)	91.61(5)
C6−Ln−O1	79.48(5)	105.07(11)
Ln−O1−Al1	101.24(5)	103.76(5)
Ln−C6−Al1	83.02(5)	85.83(5)

are somewhat elongated compared to those of the Sc−[$AlMe_4$] units in aluminate complexes $[Me_2Si(C_5H_3tBu)_2]Sc(AlMe_4)$ (Sc−C = 2.425, 2.490 Å, Sc···Al = 2.932 Å)[34] and $(C_{12}H_3Me_4iPr_2tBu)$-$Sc(AlMe_4)$ (Sc−C = 2.414, 2.442 Å, Sc···Al = 2.918 Å)[33] due to the implemented oxygen atom of the alkoxide moiety.

Similarly, the Nd−C distances of 2.698(2) Å in **3b** are slightly longer than in $Nd[AlMe_4]_3[Al_2Me_6]_{0.5}$ (2.60(1) Å)[10a,b] albeit shortened with respect to $Nd(OtBu)_3(AlMe_3)_3$ (Nd−C = 2.78(1) Å).[40] The sterically more demanding oxygen neighboring *t*Bu-groups in $Nd(OtBu)_3(AlMe_3)_3$ imply a slightly longer Nd−O distance (2.303(7) Å) than the neopentanolate ligands in **3b** (Nd−O = 2.294(1) Å).[40] The intramolecular Nd···Al distances of 3.2756(4) Å are slightly shorter compared to previously published heterobimetallic Nd/Al complexes (3.295(3)−3.411(6) Å) (Table 1, Table 2). As unambiguously evidenced by the neutron diffraction study of $Nd[AlMe_4]_3[Al_2Me_6]_{0.5}$,[10a,b] complexes **3a** and **3b** also show five-coordinate bridging carbon atoms, each with two of the hydrogen atoms tilted toward the larger Lewis-acidic metal center. Another feature that is commonly discussed for solid-state structures of homoleptic aluminates $Ln(AlMe_4)_3$ are the almost planar metallacycles $[Ln(\mu\text{-}Me)_2Al]$ defined by the metal centers and the two bridging methyl groups. Despite the fact that one of the methyl groups in **3a** and **3b** is formally displaced by oxygen, the resulting metallacycles $[Ln(\mu\text{-}Me)(\mu\text{-}O)Al]$ show a maximum deviation from the least-squares planes by only 0.106 Å (**3a**) and 0.066 Å (**3b**). The corresponding torsion angles Ln−O1−Al1−C6 are 3.95° (**3a**) and 2.62° (**3b**), respectively.

Unlike the successful $[Nd(OCH_2tBu)_3]_4 \rightarrow Nd(AlMe_4)_3$ transformation,[35] peralkylation of $Sc(OCH_2tBu)_3(AlMe_3)_3$ (**3a**) with an excess $AlMe_3$ did not afford $Sc(AlMe_4)_3$. The reaction was performed in C_6D_6 in a closed system (Teflon-valved NMR tube) to avoid any loss of side products and investigated by ^1H NMR spectroscopy. A reaction occurred only upon warming to 340 K as revealed by very slow consumption of the starting compound **3a** and formation of $[Me_2Al(\mu\text{-}OCH_2tBu)]_2$ as well as several signals between 0.8 and 1.0 ppm, assignable to mono- and bis-(alkylated) intermediates. After several hours some of these intermediate signals disappeared again. This is in contrast to the amide precursors (I and II; Scheme 1), which instantaneously reacted with $AlMe_3$. However, we could not specify the signal of the desired homoleptic $Sc(AlMe_4)_3$. This might be due to signal overlapping or most likely due to its instability in solution. Although we could not isolate any Sc tetramethylaluminate species, these findings are in agreement with a possible peralkylation of $Sc(OCH_2tBu)_3(AlMe_3)_3$ and point to the formation of such peralkylated scandium aluminate species, at least as intermediates.

Structure and Bonding of $M(AlMe_4)_3$ as Obtained from DFT Calculations. At the outset of the present study we were intrigued by the fact that several homoleptic metal(III) tetramethylaluminates $Ln(AlMe_4)_3$ of the rare earth metals were known but that we, despite the above-described efforts, were not able to isolate the putative $Sc(AlMe_4)_3$. We thus embarked on a quantum chemical investigation of such homoleptic tetramethylaluminates with the main aim to be that of uncovering the factors governing the thermodynamic stability of these compounds.

With the exception of the p-block metals, an equilibrium structure for the homoleptic tetramethylaluminate metal complex $M(AlMe_4)_3$ could be obtained for all metals investigated in this work; see Figure 2 for examples.[53−55] All optimizations of homoleptic tetramethylaluminate complexes of p-block metals (M = Al, Ga, In, Tl, and Bi) resulted instead in dissociation of the complex to yield three separate fragments, two molecules of $AlMe_3$ and the bimetallic compound $[M(Me)_3AlMe_3]$, respectively.

The DFT-optimized geometries of the existing homoleptic tetramethylaluminate rare earth metal complexes are very similar to those obtained from X-ray diffraction in general and, with the exception of La (see below), always display the same ligand

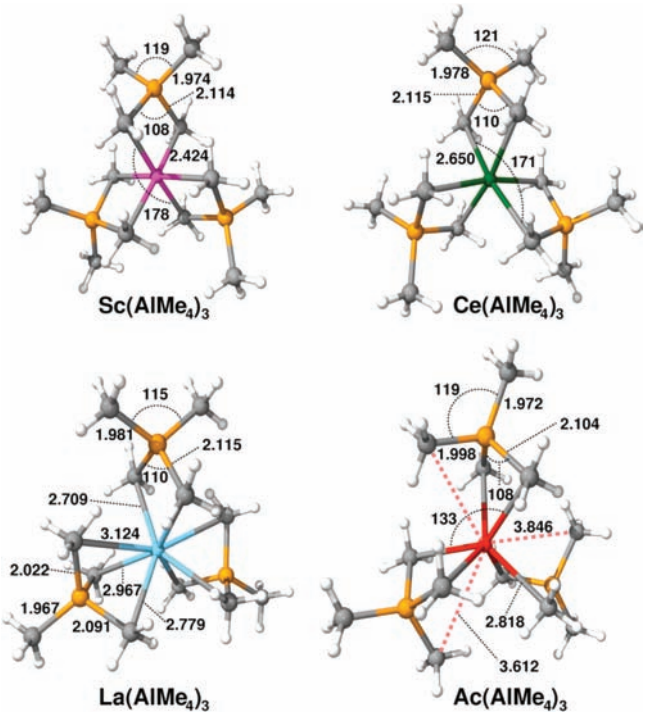

Figure 2. DFT optimized geometries of $Sc(AlMe_4)_3$ (octahedral), $Ce(AlMe_4)_3$ (distorted octahedral), $La(AlMe_4)_3$ (distorted dodecahedral, not the most stable conformation; see the text for discussion), and $Ac(AlMe_4)_3$ (distorted trigonal-prismatic, square-face tricapped). Color coding: C, gray; H, white; Al, orange; Sc, magenta; Ce, green; La, turquoise; Ac, red. Bond distances: Å. Bond angles: degree.

coordination modes as that observed in the X-ray structures. The four metal centers adopt a planar or quasi-planar configuration, the Al−Al−Al−M torsion angles being close to zero in both the X-ray and DFT structures (0−2.3°). Typically, the DFT-optimized geometry displays a root-mean-square (rms) deviation from the corresponding crystal structure of ca. 0.1 Å. For a key distance such as M···Al, the mean deviation with respect to that of the crystal structure is 0.036 Å, or only ca. 1%, for the metals La, Lu, Pr, Sm, Y, and Nd. For the largest of the metals for which a homoleptic compound $M(AlMe_4)_3$ has been structurally characterized, La and Ce, the calculations reveal a competition between coordination numbers 6 and 8. Whereas the preference in terms of calculated free energy for 6-coordination is relatively clear (3.8 (6.7) kcal/mol using M06 (B3LYP)) for Ce, consistent with the X-ray crystal structure, this preference is much smaller (1.1 (4.7) kcal/mol using M06 (B3LYP)) for La. In fact, the X-ray crystal structure of the latter compound (vide infra) shows aluminate units with coordination modes η^2-planar, η^2-bent, and η^3, respectively, resulting in an effective coordination number of at least 7. In the corresponding DFT-optimized geometry the η^2-bent, and η^3 aluminates become equivalent and show a coordination mode close to η^3, resulting in an effective coordination number approaching 8 (see Figure 2). The DFT-optimized structure is thus symmetric, with a C_2 axis passing through the lanthanum and the aluminum center of the η^2-planar aluminate, but is otherwise very similar to that of the X-ray diffraction experiment (discussed below). The failure of DFT in reproducing the preference for the higher coordination mode is very small in terms of energy, at least for the dispersion-including functional (M06), and may be due to crystal packing effects or inaccuracies in the density functionals. For the La complex, we thus chose to adopt the DFT-optimized geometry, which is closer to that of the X-ray structure, i.e., the effective 8-coordinate complex shown in Figure 2.

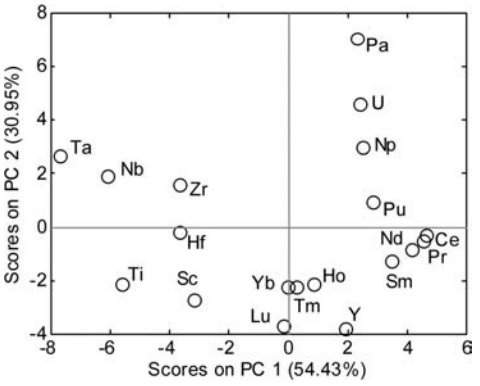

Figure 3. Score plot t1 versus t2 of the PCA of the homoleptic $M(AlMe_4)_3$ compounds.

In order to obtain an overview of the variations in geometric and electronic structure of the complexes, a set of 27 atomic (the ionic radius and electronegativity of the central metal atom) and molecular (geometric and electronic properties calculated for the homoleptic complexes) descriptors were prepared and applied in a principal component analysis (PCA).[56] The complete list of descriptors is given in the Supporting Information. Based on cross-validation and the eigenvalue plot,[57] three principal components (PCs) were retained in the model. Q residuals and Hotelling's T^2 statistics[58] revealed the presence of three unusual samples (M = La, Th, and Ac) that were not included in the model. The DFT-optimized geometries of these metal complexes deviate considerably from those of the other metals and are the main reason why these metals should be considered as outliers and excluded from the model. For example, whereas the central metal atom in all other complexes is hexacoordinate, with the three tetramethylaluminate ligands in an η^2 "edge coordination" fashion (see, e.g., the structure of $Ce(AlMe_4)_3$ in Figure 2), the large cation size of Ac^{3+}, Th^{3+}, and La^{3+} also allows for a η^3 "face coordination" of the aluminate, resulting in a metal coordination number higher than 6. For lanthanum and thorium in particular, two of the ligands are face-coordinated and the third edge-coordinated. For actinium, the binding mode of all three ligands are intermediate between edge and a face, with one of the Ac−methyl bond distances being 0.8−1.0 Å longer than the others (Figure 2).

The new PCA model based on the remaining 19 complexes does not contain outliers; see Figure 3 and Figure 4 for the scores and loading plots, respectively. Two principal components, explaining 85.4% of the total variance, were retained and used in a *k*-means nearest group cluster analysis[56] employing the Mahalanobis distance;[59] see the dendrogram in Figure 5. Whereas the loadings of PC1 (Figure 4) mainly are characterized by descriptors related to the size (descriptors 1−3, 5−9, and 21−25) and electronegativity (4) of the metal center, the descriptors related to the nature (ionic or covalent) of the bond between the metal center and the tetramethylaluminate ligands (12, 13, 15, 16, 18−20) dominate PC2. See the Supporting Information for the definition of the descriptors.

The dendrogram shown in Figure 5 reveals three main clusters. The largest cluster (in the middle) contains the rare

dx.doi.org/10.1021/ja2001049 |*J. Am. Chem. Soc.* 2011, 133, 6323–6337

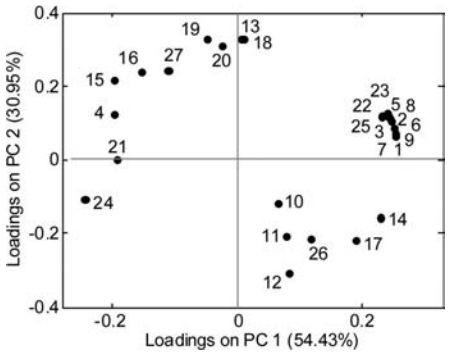

Figure 4. PCA loadings plot p1 versus p2. The numbers are those of the descriptors, defined in the Supporting Information.

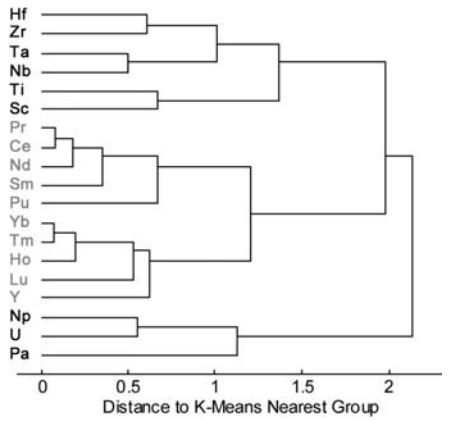

Figure 5. Dendrogram illustrating the cluster analysis.

earth metal complexes (except that of scandium) in addition to the complex of the smallest actinide included in our set, plutonium. Many of these metals have already been observed to form homoleptic tetramethylaluminate complexes. With the exception of plutonium, the Allred–Rochow electronegativity of these elements is below 1.15. Their ionic radii range from medium (Yb, Tm, Ho, Lu, and Y) to large (Pr, Ce, Nd, Sm, and Pu), reflected by the presence of two subclusters. The M–($AlMe_4$) bond in these complexes is essentially ionic. For most of these complexes, the best Lewis structure arrived at in natural bond orbital (NBO) analysis[60] is that of a M^{3+} ion surrounded by three $[Al(CH_3)_4]^-$ ions. The absence or low number of three-center two-electron M–C–Al bonds detected in the NBO analysis is a further indication that most of these metal–methylaluminate bonds are fairly ionic, see Table 3. Some tendency toward formation of three-center two-electron M–C–Al bonds, and thus of covalency, is seen for M = Pu, Sm, Y, and Lu, as well as for La (which was excluded from the PCA model), but the ionic model still appears to be the best approximation even for these complexes since the delocalized bonds either remain in minority or are quite polarized toward tetramethylaluminate.[61]

The smallest cluster (lower part of the dendrogram) contains the complexes of three early actinides (Np, U, and Pa). These metals are characterized by large ionic radii, electronegativities that are generally higher than those of the corresponding lanthanides, as well as significant contribution from 5f in the valence bonding orbitals. Thus the M–($AlMe_4$) bonds are more covalent than those of the lanthanides, as

Table 3. Three-Center Two-Electron (M–C–Al) Bonds in the $M(AlMe_4)_3$ Complexes

		open shell[a]		
M	closed shell[a]	α spin	β spin	M cn[b]
Ti	6 (9.0)			6
Zr		4 (12.3)	6 (9.5)	6
Hf		3 (11.6); 2 Hf–C bonds[c]	6 (8.7)	6
Nb		2 (9.8); 3 Nb–C bonds[c]	6 (11.3)	6
Ta		2 (11.5); 3 Ta–C bonds[c]	6 (8.7)	6
Sc	6 (8.0)			6
Y	6 (6.0)			6
Ho		0	0	6
Tm		0	0	6
Yb		0	0	6
Lu	6 (6.7)			6
La	7 (6.8)			8
Ce		0	0	6
Pr		0	0	6
Nd		0	0	6
Sm		2 (11.0)	0	6
Ac	6 (6.6)			9
Th		6 (11.7)	8 (10.9)	8
Pa		6 (11.8)	6 (11.3)	6
U		6 (11.2)	6 (10.5)	6
Np		4 (11.1)	0	6
Pu		4 (10.8)	0	6

[a] Number of three-center bonds (averaged percentage of metal character) as identified using NBO.[60] [b] Coordination number of the metal M. [c] Two-center natural bond.

evident from the delocalized bonds in Table 3, and the covalency increases with the extension of the 5f orbitals (Np < U < Pa).[62,63]

The covalent contributions to the M–($AlMe_4$) bonds are also significant for the complexes of the third cluster (at the top), which contains all of the transition metal complexes as well as that of the smallest rare earth element (scandium). Scandium thus groups together with titanium and not, as one might expect, with lutetium or yttrium, and the PCA suggests that this contrast to the other rare earth elements mainly results from the smaller ionic radius and higher electronegativity of scandium. The covalency of the M–($AlMe_4$) bonds appears to increase with both the metal electronegativity and the cation size (Sc < Ti < Zr, Hf < Nb, Ta), see Table 3. The increase in covalency upon going from titanium to zirconium may, at first glance, seem puzzling since titanium is both the smallest and most electronegative of the two. However, vertical trends in transition metal chemistry often originate from the relative energies and spatial extensions of the metal valence s and d orbitals.[64] Valence 4d and 5d orbitals are less compact and more suitable for sd hybrid orbital formation than are valence 3d orbitals. For example, the ratio between ns and $(n - 1)$d radial expectation values is in the range 2.49–2.50 for titanium and significantly lower for zirconium and hafnium (1.81–183 and 1.53–158, respectively).[62]

The covalent contributions seen for both the actinide- and the transition-metal cluster imply that the simple ionic bonding model that worked well for the lanthanides (the largest cluster) turns out to be inadequate for the description of most of the

Scheme 3. Loss of $Al(CH_3)_3$ from the Homoleptic Tetramethylaluminate Metal(III) Complex

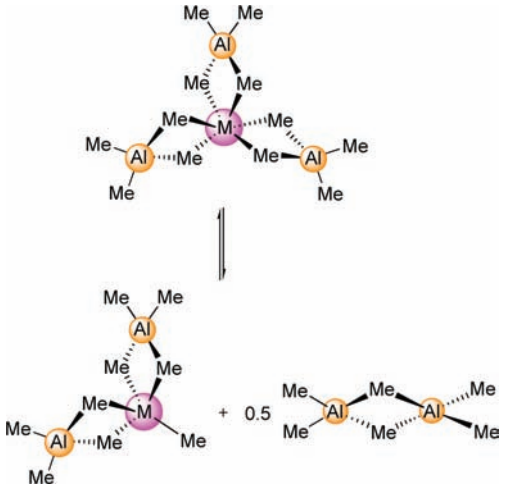

Table 4. Calculated Free Energies for the Loss of Trimethylaluminum from the Homoleptic Metal(III) Tetramethylaluminate Complex in Heptane at 298.15 K[a]

	B3LYP	M06		B3LYP	M06
Ti	−15.2	−6.7	La	−2.9	9.1
Zr	−7.6	1.2	Ce	1.3	10.0
Hf	−9.1	0.1	Pr	−0.7	7.4
Nb	−12.3	1.5	Nd	−0.7	7.8
Ta	−14.6	−0.5	Sm	−1.4	6.4
Sc	−8.7	−0.4	Ac	2.1	12.7
Y	−2.1	6.0	Th	−5.8	7.8
Ho	0.6	8.2	Pa	−0.4	8.7
Tm	−3.0	6.3	U	0.6	9.2
Yb	−2.3	6.9	Np	−1.3	7.6
Lu	−3.1	5.7	Pu	−2.4	6.8

[a] The reaction is shown in Scheme 3. The reaction energies are given in kilocalories per mole.

complexes of the other two clusters. Instead, in these compounds the bonds between the metal and the tetramethylaluminates are, in general, better described by three-center two-electron M−C−Al bonds in which the contributions from the metal M and Al are of similar magnitude (9−12% for M, and 12−15% for Al).

Thermodynamic Stability of the $M(AlMe_4)_3$ Complexes. As already mentioned, no minima pertaining to homoleptic tetramethylaluminate complexes could be located for the p-block metals (M = Al, Ga, In, Tl, and Bi). These geometry optimizations resulted in dissociation to yield two molecules of $AlMe_3$ and the bimetallic compound $[MMe_2(AlMe_4)]$, respectively. This suggests that loss of trimethylaluminum could represent a useful measure for the stability of the homoleptic tetramethylaluminate complexes (Scheme 3).

We have calculated the reaction energy for the dissociation in Scheme 3 using three different density functionals: the generalized-gradient approximation (GGA) functional BPW91,[65] the hybrid-GGA functional B3LYP,[66] and the hybrid meta-GGA functional M06.[67] The stabilities of the homoleptic complexes obtained using BPW91 (see the Supporting Information) and the hybrid-GGA functional B3LYP (Table 4) are very similar, and it is gratifying that the recently developed hybrid functional M06 (Table 4) offers a trend similar to that predicted by the two more well-tested functionals. M06 predicts stabilities that are systematically higher than those of the two other functionals, and this difference is attributed to the fact that this functional has been constructed to account for medium-range correlation and attractive noncovalent interactions (dispersion), effects not included in BPW91 and B3LYP. This suggests that, among the three functionals included in the present work, M06 is taken to offer the most accurate absolute stabilities. In fact, the M06 relative free energies in solution (heptane)[68] for the rare earth metals for which tetramethylaluminates $M(AlMe_4)_3$ have so far been characterized (M = Y, La, Ce (**4a**), Pr, Nd, Sm, Ho, Tm (**4b**), Yb (**4c**) and Lu)[10c,d,36] are all clearly positive and indicate stability. In contrast, the homoleptic tetramethylaluminate of scandium, which has proven difficult to achieve, has a slightly negative relative free energy (M06, heptane) and markedly lower than the rare earth elements for which homoleptic tetramethylaluminate complexes are known. Similarly, the stabilities of the transition metal complexes also do not seem promising with respect to obtaining stable homoleptic complexes. In contrast, all actinides included in the present study are predicted to give homoleptic compounds with stabilities comparable to those of the rare earth metals for which such complexes are known.

In order to investigate the factors governing the stability of the homoleptic compounds, the free energy change of the reaction (Scheme 3) in heptane[68] as calculated using the M06 functional was correlated in a partial least-squares regression (PLSR)[56] model involving 27 molecular descriptors (independent variables). We started to build a model containing the entire set of tetramethylaluminate complexes, and using standard multivariate procedures,[57] two unusual samples (Ti and Th) were detected and removed from the calibration model.[69]

To evaluate the error of the model, the leave-one-out root-mean-square error of cross validation (RMSECV) was employed. Accordingly, the model based on one factor was found to be the most predictive. This model explained 50.6% of the **X**-block and 83.4% of the variance in **y**. The respective RMSECV was 1.8 kcal/mol, corresponding to 13.4% of the calibration range (13.2 kcal/mol). We proceeded to improve the model by performing a manual pruning of the descriptors. This work involves removing from the model, one after the other, those descriptors that are strongly correlated to each other, as well as those that contribute only little to the multivariate model. After each pruning a new PLS model was established, and the predictive ability of the model was evaluated by means of the corresponding RMSECV. In the final, superior model, only the two atomic descriptors, the Allred−Rochow electronegativity of the central metal atom (descriptor 4) and the effective ionic radius M^{3+} (descriptor 25), were retained. Using two factors, the explained variance in **y** is 90.7% and the RMSECV 1.3 kcal/mol, which corresponds to 9.8% of the calibration range. The standardized regression coefficients (β weights) were −0.27 (descriptor 4) and 0.77 (descriptor 25), respectively. This smaller model is both more predictive and easier to interpret than the initial model.

First, the negative correlation between the electronegativity of the central metal atom (descriptor 4) and the stability of the complex confirms that ionic metal−tetramethylaluminate interactions are to a large extent determining the stability of the homoleptic compounds. In other words, electropositive central

dx.doi.org/10.1021/ja2001049 |J. Am. Chem. Soc. 2011, 133, 6323–6337

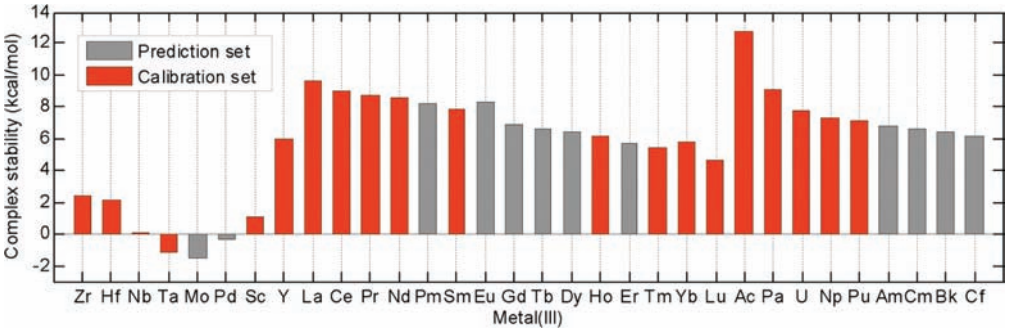

Figure 6. Predicted stability toward loss of trimethylaluminum, as defined in Scheme 3, for homoleptic metal(III) tetramethylaluminates.

metal atoms stabilize the homoleptic compounds toward loss of trimethylaluminum, which again reflects the observation that such compounds have so far been obtained only for low-electronegativity rare earth metals (vide supra).[10c,d,36] An increasing electronegativity of the central metal atom not only decreases the ionic metal−tetramethylaluminate interactions but also weakens the aluminum−methyl bonds of the tetramethylaluminate ligands[70] and thus reduces their stability toward loss of trimethylaluminum and formation of two more covalent compounds, $(AlMe_4)_2M\text{-}CH_3$ and Al_2Me_6, see Scheme 3.

Neptunium and cerium are examples of the effect of electronegativity in that these ions are of the same size (effective ionic radius 1.01 Å) and form homoleptic compounds with similar distorted octahedral geometries. However, their Allred−Rochow electronegativities are different (1.22 and 1.08, respectively), resulting in a 2.4 kcal/mol lower calculated stability for the neptunium complex.

Second, the main prerequisite for obtaining a stable homoleptic complex is simply that the central metal cation be sufficiently large (descriptor 25). Indeed, the cationic radius is strongly positively correlated with the stability of the homoleptic complex ($R^2 = 0.88$). Of course, it is difficult to separate simple size effects from those of electronegativity. However, the steric exchange repulsion calculated between the tetramethylaluminate groups correlates negatively with stability of the homoleptic complexes ($R^2 = 0.81$) suggesting that some of the influence of ionic size simply is one of reducing the steric repulsion between the tetramethylaluminate groups. For example, upon going from Ac (ionic radius 1.12 Å) to Ti (0.67 Å),[71] the calculated steric repulsion between the four tetramethylaluminate ligands increases from 27 to 114 kcal/mol and renders the homoleptic complex less stable toward loss of a $AlMe_3$ molecule. This hypothesis is also supported by the fact that tetramethylaluminate face coordination (η^3), which should minimize the distance and maximize the electrostatic attraction between the central cation and the center of the $[AlMe_4]^-$ anion, is observed only for the largest cations such as lanthanum, thorium, and actinium; see Figure 2.

By the same token one might expect the η^1 coordination mode, which is the sterically least demanding and which maximizes the distance between the central cation and the $[AlMe_4]^-$ anion, to be preferred for small cations such as Sc^{3+}. However, attempts to optimize the geometry of $Sc(AlMe_4)_3$ using a η^1 coordination mode for one of the aluminate ligands resulted in the loss of trimethylaluminum and formation of $(AlMe_4)_2Sc\text{-}CH_3$.

An important advantage of our simple PLSR model is that both descriptors are available for most metals with a stable oxidation state +3. Thus, the calibration model can be used, without additional cost, to estimate the stability and predict the existence of other metal(III) tetramethylaluminate homoleptic complexes; see Figure 6. We have considered only elements for which the values of both descriptors are within the respective calibration ranges.

All lanthanides and actinides are predicted to provide homoleptic complexes that are stable toward loss of trimethylaluminum, including compounds of both early, e.g., Ce, and late, e.g., Tm and Yb, lanthanides not previously reported. Other competing reactions are not considered in the current model. For example, for some metals the low stability of oxidation state +3 may hamper formation and isolation of the homoleptic complex. This may be the case for europium and ytterbium, for which our model predicts stable homoleptic compounds, but which are known to be Ln^{3+}/Ln^{2+} redox-active.

In conclusion, low electronegativity and a sufficiently large cation are required for the central metal atom to provide stable homoleptic tetramethylaluminate complexes. These two features are common to all rare earth elements for which the homoleptic complex has been obtained and structurally characterized. Scandium, on the other hand, has a small cation and is sufficiently electronegative so as to render the corresponding homoleptic complex thermodynamically unstable toward loss of trimethylaluminum. The same arguments can be used to predict low stability for the corresponding complexes of most or perhaps even all transition metals. Finally, mainly because of their size, all the actinides considered here are predicted to give stable homoleptic compounds despite their electronegativities generally being somewhat higher than those of the lanthanides.

Synthesis of $Ce(AlMe_4)_3$. The cerium derivative **4a** was synthesized previously following route I (Scheme 1).[10d] We revisited this compound for examining its solid-state structure in order to demonstrate the predictive capability of the DFT studies and to expand into any Ce^{4+}/Ce^{3+} aluminate chemistry. From a structural point of view, it was interesting to see whether **4a** would adopt a solid-state structure similar to La or Pr. The homoleptic trivalent lanthanides show different crystallization behavior depending on the Ln^{3+} size and the temperature (vide infra). $La(AlMe_4)_3$, containing the largest central ion in this series, crystallizes in the monoclinic space group $P2_1/n$ with one molecule in the asymmetric unit.[10d] This compound exhibits three different aluminate coordination modes in the solid state comprising a η^2-planar, η^2-bent, and η^3 one. Interestingly, when this geometry is optimized at DFT level, the number of different coordination modes is reduced to two. Indeed, whereas the η^2-planar-type ligand is reproduced, the spatial orientation relative to the metal center of the other ligands becomes equivalent and intermediate to those of the η^2-bent- and η^3-type

dx.doi.org/10.1021/ja2001049 |J. Am. Chem. Soc. 2011, 133, 6323–6337

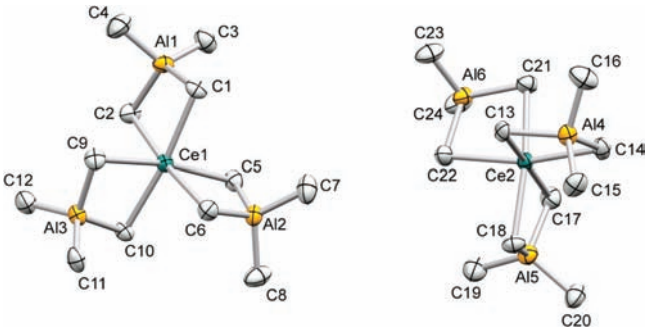

Figure 7. Two independent molecules in the solid-state structure of $Ce(AlMe_4)_3$ (**4a**). Anisotropic displacement parameters are drawn at the 50% probability level.

ligands, albeit closer to that of the latter. The DFT-optimized structure is symmetric, having one C_2 axis that passes through the lanthanum and the aluminum center of the η^2-planar-type ligand.

Homoleptic aluminates of the slightly smaller Ln^{3+} ions (Ln = Pr, Nd) crystallize in the monoclinic space group $P2_1/a$ with two independent molecules per unit cell. Finally, $Sm(AlMe_4)_3$, $Y(AlMe_4)_3$, and $Lu(AlMe_4)_3$, representing the midsized to small Ln^{3+} ions, crystallize in the centrosymmetric space group $C2/c$ with one independent molecule per unit cell. Crystals of **4a** were grown from saturated hexane solutions at −35 °C, displaying the same crystal system as Pr and Nd ($P2_1/a$). Each of the three $[AlMe_4]^-$ ligands coordinates via two methyl groups that bridge in a η^2 fashion to the central metal, accomplishing a pseudo-octahedral geometry (Figure 7, Table 5) in excellent agreement with the coordination mode predicted by DFT (see Figure 2). Interestingly, the two independent molecules in the unit cell show distinct geometries of the $[Ce(\mu\text{-}Me)_2Al]$ metallacycles. Although in molecule 1 the maximum deviation from planarity is 1.2(3)° (Ce1−C9−Al1−C10) for the three metallacycles, molecule 2 reveals one reasonably planar moiety with a torsion angle of 2.75° and two significantly distorted ones (torsion angles 9.49° and −10.28°). This feature, which is equivalent to a bending of the tetramethylaluminate ligand, is more pronounced in **4a** than in the Pr and Nd derivatives, in agreement with the increased size of the Ln^{3+} center.[10d] The Ce−C(μ-Me) bonds are slightly longer than observed for the Pr derivative (av 2.628/2.635 vs 2.606/2.606 Å)[10d] consistent with the larger metal center.

Synthesis of $Tm(AlMe_4)_3$. The thulium derivative **4b** was synthesized according to equation I (Scheme 1) and obtained in 51% crystalline yield from saturated hexane solutions at −35 °C. The composition was unequivocally proven by X-ray structure analysis (Figure 8). Derivative **4b** is isomorphous ($C2/c$) to $Ln(AlMe_4)_3$ representing the mid- (Ln = Sm) and smaller-sized rare earth metals (Ln = Y, Lu). The torsion angles Tm1−C1−Al1−C2 of the $[Tm(\mu\text{-}Me)_2Al]$ metallacycles were in the range 0−0.26°, only slightly below that predicted (0.16−0.47°) by DFT. Consistent with the lanthanide contraction, the average of the Ln−C(μ-Me) distance in **4b** was 2.485 Å (close to that (2.516 Å) predicted by DFT), i.e., slightly longer than that of $Lu(AlMe_4)_3$ (2.464 Å (X-ray), 2.495 Å (DFT)) (Table 5).[10d]

Attempted Synthesis of $Eu(AlMe_4)_3$. Given the reducing power of organoaluminum compounds,[72] we were curious whether trivalent derivatives $Ln(AlMe_4)_3$ of europium (E^0 (Eu^{2+}/Eu^{3+}) = −0.36 V) and ytterbium (E^0 (Yb^{2+}/Yb^{3+}) = −1.15 V) are isolable. Europium(III) and ytterbium(III) are more prone to be reduced to the divalent state than samarium

Table 5. Selected Bond Lengths [Å] and Angles [deg] in Compounds 4a, 4b, and $4c^{LT}$

$Ce(AlMe_4)_3$ (**4a**)			
molecule1		molecule 2	
Ce1−C1	2.623(7)	Ce2−C13	2.635(7)
Ce1−C2	2.620(7)	Ce2−C14	2.626(8)
Ce1−C5	2.631(8)	Ce2−C17	2.646(8)
Ce1−C6	2.643(7)	Ce2−C18	2.646(7)
Ce1−C9	2.628(7)	Ce2−C21	2.637(7)
Ce1−C10	2.620(7)	Ce2−C22	2.621(8)
Al1−C1	2.080(7)	Al4−C13	2.071(8)
Al1−C2	2.083(7)	Al4−C14	2.082(8)
Al1−C3	1.959(9)	Al4−C15	1.958(8)
Al1−C4	1.970(11)	Al4−C16	1.952(12)
Ce1···Al1	3.196(2)	Ce2···Al4	3.194(2)
Ce1···Al2	3.215(2)	Ce2···Al5	3.219(2)
Ce1···Al3	3.188(2)	Ce2···Al6	3.179(2)
C1−Ce1−C2	80.9(2)	C13−Ce2−C14	80.2(2)
C1−Ce1−C5	92.1(2)	C13−Ce2−C17	175.3(2)
C1−Ce1−C6	95.5(2)	C13−Ce2−C18	96.4(2)
C1−Ce1−C9	95.6(2)	C13−Ce2−C21	92.8(2)
C1−Ce1−C10	172.2(2)	C13−Ce2−C22	88.7(3)
C1−Al1−C2	109.5(3)	C13−Al4−C14	109.4(3)
C1−Al1−C3	108.6(3)	C13−Al4−C15	107.1(4)
C1−Al1−C4	105.5(4)	C13−Al4−C16	105.1(4)
C3−Al1−C4	120.2(5)	C15−Al4−C16	119.3(5)
$Tm(AlMe_4)_3$ (**4b**)		$Yb(AlMe_4)_3$ ($4c^{LT}$)	
Tm−C1	2.488(2)	Yb−C1	2.465(2)
Tm−C2	2.491(2)	Yb−C5	2.477(3)
Tm−C5	2.477(2)	Yb−C6	2.480(4)
Al1−C1	2.088(2)	Al1−C5	2.072(3)
Al1−C2	2.083(2)	Al1−C6	2.084(3)
Al1−C3	1.967(2)	Al1−C7	1.953(4)
Al2−C5	2.093(2)	Al1−C8	1.956(5)
Al2−C6	1.960(2)	Al2−C1	2.083(2)
		Al2−C3	1.953(6)
Tm···Al1	3.0407(5)	Yb···Al1	3.0242(7)
Tm···Al2	3.0290(6)	Yb···Al2	3.0124(11)
C1−Tm−C2	85.74(4)	C1−Yb−C1′	86.55(8)
C1−Tm−C5	92.17(4)	C1−Yb−C5	91.52(9)
C1−Tm−C5′	89.25(4)	C1−Yb−C6	91.9(1)
C5−Tm−C5′	86.51(6)	C5−Yb−C6	85.9(1)
C1−Al1−C2	108.64(5)	C5−Al1−C6	108.7(1)
C5−Al2−C5′	108.35(7)	C1−Al2−C1′	108.4(1)
C3−Al1−C4	118.55(7)	C7−Al1−C8	118.6(2)
C6−Al2−C6′	119.5(2)	C3−Al2−C3′	119.3(2)

(E^0 (Sm^{2+}/Sm^{3+}) = −1.55 V) or even thulium(III) (E^0 (Tm^{2+}/Tm^{3+}) = −2.1 V).[73] In the case of europium, route I (Scheme 1) yielded an off-white precipitate and a colorless hexane solution devoid of any rare earth metal component. Apparently, complete reduction and formation of insoluble $[Eu^{2+}(AlMe_4)_2]_n$ (**5a**) occurred, coprecipitating with LiCl. To further investigate into this reactivity and to be able to isolate pure **5a**, we followed reaction protocol II (Scheme 1). Accordingly, compound **5a** could be isolated

dx.doi.org/10.1021/ja2001049 |J. Am. Chem. Soc. 2011, 133, 6323–6337

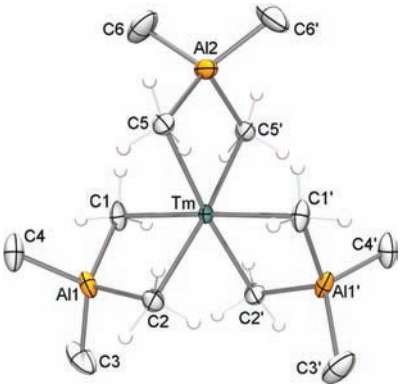

Figure 8. Solid-state structure of $Tm(AlMe_4)_3$ (**4b**). Anisotropic displacement parameters are drawn at the 50% probability level.

Scheme 4. Formation of $[Eu^{2+}(AlR_4)_2]_n$ (R = Me (5a), Et (5b)) from the Trivalent Europium Silylamide Complex 2a

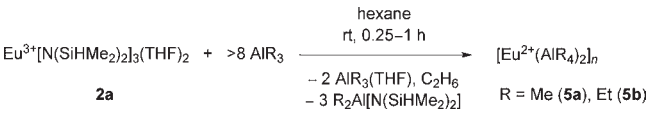

Scheme 5. Thermally Induced "Self-Reduction" of Yb$(AlMe_4)_3$ (4c)

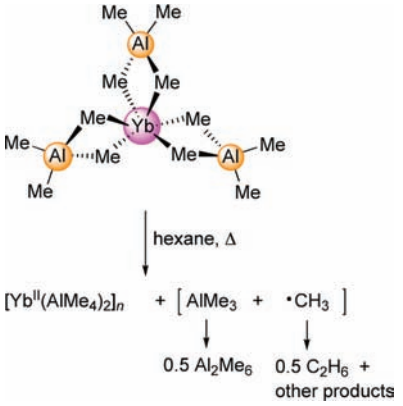

and characterized by FTIR spectroscopy and elemental analysis. This specific redox reaction was further proven by addition of $AlEt_3$ instead of $AlMe_3$ yielding the hexane-soluble ethyl derivative $[Eu^{2+}(AlEt_4)_2]_n$ (**5b**) (Scheme 4). Light green crystals of **5b** suitable for X-ray structure analysis were grown from a saturated hexane solution at −35 °C. Complex **5b** crystallizes in the trigonal space group $P3_2$, being isotypic to the polymeric network structures of $[M^{2+}(AlEt_4)_2]_n$ (M = Sm, Yb, Ca).[8d,11] Further information concerning structural parameters of **5b** can be obtained from the Supporting Material (Figure S1).

Synthesis and Reduction Behavior of Yb$(AlMe_4)_3$. In contrast to europium, the trivalent ytterbium and samarium derivatives $Ln(AlMe_4)_3$ (Ln = Sm,[10d] Yb (**4c**)) can be isolated according to route I (Scheme 1). The crystallized yields for ytterbium are low (ca. 20%), since reduction to the divalent species is prevailing when the alkylation reaction is performed at ambient temperature.

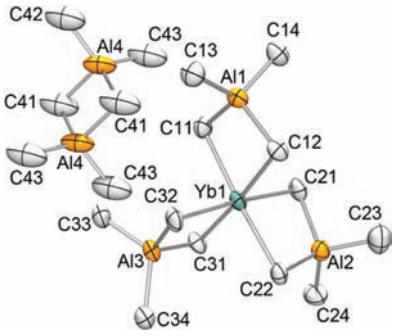

Figure 9. Solid-state structure of $Yb(AlMe_4)_3 \times (Al_2Me_6)_{0.5}$ (**4c′**). Anisotropic displacement parameters are drawn at the 50% probability level. For selected bond distances, see Supporting Information.

Better yields are also hampered due to the necessary separation of trimethylaluminum from initially crystallized $Yb(AlMe_4)_3 \times (Al_2Me_6)_{0.5}$ (**4c′**).[10a,b] Moreover, synthesis and isolation of **4c** applying reaction protocol II and $Yb[N(SiHMe_2)_2]_3(THF)_2$ (**2b**) (Figure S2 in Supporting Information) as a precursor was less straightforward due to the complicated separation of coproduct $[\{Me_2AlN(SiHMe_2)_2\}_2]$; however, reduction to the divalent species was also observed. $Yb(AlMe_4)_3$ (**4c**) can be stored without reduction in solid form at −30 °C; however, precipitation of yellow $[Yb(AlMe_4)_2]_n$[11a] occurs instantaneously when a hexane solution of the pure crystallized compound is kept at ambient temperature (Scheme 5).

Such $Ln(AlMe_4)_3 \rightarrow [Ln(AlMe_4)_2]_n$ "self-reductions" are favored at elevated temperature and were examined in more detail by FTIR (Figure S8) and NMR spectroscopy. The formation of both Al_2Me_6 and ethane is unambiguously evidenced by ^1H NMR spectroscopy. Taking into account the concurrent formation of CH_4, CH_3D, and $CH_3C_6D_5$ (in benzene-d_6, Figure S6) and CH_4, CH_3D (in cyclohexane-d_{12}, Figure S7), reduction of the Yb^{3+} center via methyl radical formation is suggested (Scheme 5). Also shown in the Supporting Information are the variable temperature ^1H NMR spectra of **4c** in toluene-d_8 (Figure S5), revealing a decoalescence of the methyl resonance at ca. 298 K (cf., Lu: 278 K, Y: 229 K, Sm: 216 K).

The solid-state structure of $Yb(AlMe_4)_3$ was examined in detail by multiple X-ray structure analyses. As shown previously for the yttrium and neodymium derivatives,[10a,b] crystallization of the supernatant hexane solutions, obtained according to eq I (Scheme 1), yielded $Yb(AlMe_4)_3 \times (Al_2Me_6)_{0.5}$ (**4c′**, Figure 9). "$AlMe_3$-free" **4c** is produced when **4c′** is exposed to vacuum. Interestingly, the initial X-ray diffraction study of **4c** (denoted as $\mathbf{4c}^{HT}$, HT= high temperature), performed at 213 K revealed a monoclinic crystal system with space group $P2_1/c$ (Figure S3), thus isostructural with those of the larger rare earth metal centers (cf., Ce (**4a**) T = 100 K). The effect of temperature was evident when the crystal data for **4c** were collected at 173 K ($\mathbf{4c}^{LT}$, LT = low temperature, Figure S4), showing the expected space group $C2/c$ found previously for the small rare earth metal centers at the same or lower temperature (cf., Tm(**4b**)). The Yb−C bond lengths in $\mathbf{4c}^{LT}$ (av 2.474 Å, Table), $\mathbf{4c}^{HT}$ (av 2.485 and 2.477 Å), and **4c′** (av 2.495 Å) are similar and also compare very well with the corresponding distance (2.508 Å) obtained from DFT. The [Yb(μ-Me)$_2$Al] metallacycles show similar maximum deviation from planarity (the Yb−μ-C−Al−μ-C torsion angles being 0.00°/−0.05°/−0.05° versus 2.79°/−1.76°/0.14/° and 1.14°/−1.79°/1.48° versus 1.48°/1.73°/−2.56°, again comparing

dx.doi.org/10.1021/ja2001049 |J. Am. Chem. Soc. 2011, 133, 6323–6337

very well with the corresponding ones (−0.23°/0.12°/−0.33°) from DFT), comparable to those of the thulium (**4b**) and lutetium derivatives.

As a result of the more negative redox potential, the samarium congener is relatively stable; however, yellow hexane solutions of $Sm(AlMe_4)_3$ also gradually produce purple insoluble $[Sm(AlMe_4)_2]_n$[11b] over time and upon heating.[74]

CONCLUSIONS

Complexes $[Ln(OCH_2tBu)_3]_4$ give straightforward access to scandium and neodymium neopentanolate trimethylaluminum adducts that are of relevance for olefin polymerization. Such compounds of the larger lanthanide metal centers might also be exploited for continuative alkylation reactions. However, the smallest rare earth metal scandium strengthened again its prominent position. Our investigations regarding the reactivity of $Sc(OCH_2tBu)_3(AlMe_3)_3$ toward $AlMe_3$ point at a peralkylated species, but we still were not able to unambiguously characterize $Sc(AlMe_4)_3$.

Multivariate classification and modeling of a variety of tetramethylaluminates $M(AlMe_4)_3$ and their stability based on quantum chemically obtained relative energies and atomic and molecular descriptors have identified low electronegativity and a sufficiently large ionic radius for the central metal atom as essential factors for obtaining homoleptic compounds stable toward loss of trimethylaluminum, the presumed main decomposition reaction. The fact that the preparation and characterization of $Sc(AlMe_4)_3$ have proven very challenging, despite great efforts in this and previous studies, is reflected in the finding that scandium is too small and too electronegative to form a stable homoleptic compound. In contrast, a series of new homoleptic compounds based on lanthanides and actinides are predicted to be stable toward loss of trimethylaluminum. Three of the predicted lanthanide-based compounds $Ln(AlMe_4)_3$ (Ln = Ce, Tm, Yb) have been prepared and fully characterized in the present work, in addition to $Ln(OCH_2tBu)_3(AlMe_3)_3$ (Ln = Sc, Nd), and $[Eu(AlEt_4)_2]_n$. At ambient temperature, donor-free hexane solutions of $Ln(AlMe_4)_3$ of the Ln^{3+}/Ln^{2+} redox-active metal centers display enhanced reduction to $[Ln(AlMe_4)_2]_n$ with decreasing negative redox potential, in the order Eu ≫ Yb ≫ Sm. Whereas $Eu(AlMe_4)_3$ could not be identified, $Yb(AlMe_4)_3$ turned out to be isolable in low yield.

EXPERIMENTAL DETAILS

General Procedures. All operations were performed with rigorous exclusion of air and water, using standard Schlenk, high-vacuum, and glovebox techniques (MBraun MB200B; <1 ppm O_2, <1 ppm H_2O). Hexane was purified using Grubbs columns (MBraun SPS, solvent purification system). Benzene-d_6, toluene-d_8, and cyclohexane-d_{12} were obtained from Aldrich, degassed, dried over Na for 24 h, filtered, and stored in a glovebox. $AlMe_3$ and $AlEt_3$ were purchased from Aldrich and used as received. **CAUTION:** Alkylaluminum reagents react violently with moisture. $LnCl_3$ (Ln = Ce, Eu, Tm, Yb) were obtained from Strem Chemicals and activated with THF. Complexes $Ln[N(SiMe_3)_2]_3$,[51,75] $Ln[N(SiHMe_2)_2]_3(THF)_x$,[76] $[Nd(OCH_2tBu)_3]_4$,[38] $Nd(OCH_2tBu)_3(AlMe_3)_3$ (**3b**),[39] and $Ln(AlMe_4)_3$ (Ln = Sm, Ce)[10d] were synthesized according to previously published procedures. NMR spectra were recorded at 25 °C on a Bruker-AVANCE-DMX400 (^1H, 400.13 MHz; ^{13}C, 100.62 MHz), and a Bruker−BIOSPIN-AV500 (5 mm BBO; ^1H, 500.13 MHz; ^{13}C, 125.77 MHz). ^1H and ^{13}C shifts are referenced to internal solvent resonances and reported in parts per million relative to TMS. IR spectra were recorded on a Nicolet-Impact 410 FTIR spectrometer as Nujol mulls sandwiched between CsI plates. Elemental analyses were performed on an Elementar Vario EL III.

$[Sc(NMe_2)_3(LiCl)_3]$ (1a) and $[Sc(OCH_2tBu)_3]_4$. A THF solution of 3 equiv of $LiNMe_2$ (208 mg, 4.08 mmol) was added slowly to a suspension of $ScCl_3(THF)_3$ (500 mg, 1.36 mmol) in THF, and the mixture was stirred at ambient temperature for 18 h. The solvent was then removed in vacuo until dryness. The remaining solid was suspended in hexane, 3 equiv of neopentanol (360 mg, 4.08 mmol) in hexane was added, and the resulting mixture was stirred at ambient temperature. After 1 h the solvent was removed under reduced pressure, the residue was extracted several times with hexane, and the tetranuclear alkoxide complex (560 mg, 1.07 mmol, 79%) was separated by crystallization at −35 °C. The analytical data are consistent with the literature known compound synthesized from $Sc[N(SiMe_3)_2]_3$.[38]

$Eu[N(SiHMe_2)_2]_3(THF)_2$ (2a). Following the procedure described previously[76] $EuCl_3(THF)_{3.5}$ (409 mg, 0.80 mmol) and $Li[N(SiHMe_2)_2]$ (323 mg, 2.32 mmol) yielded **2a** as dark red crystals (252 mg, 0.36 mmol, 45%). ^1H NMR (400.13 MHz, benzene-d_6): δ 11.76 (br s, *THF*), 4.69 (6 H, Si*H*), 0.08 (s, 36 H, Si*Me*$_2$) ppm.

$Yb[N(SiHMe_2)_2]_3(THF)_2$ (2b). Following the procedure described previously[76] $YbCl_3(THF)_3$ (397 mg, 0.80 mmol) and $Li[N(SiHMe_2)_2]$ (323 mg, 2.32 mmol) yielded **2b** as colorless crystals (302 mg, 0.42 mmol, 53%). ^1H NMR (400.13 MHz, benzene-d_6): δ 4.61 (s, 6 H, Si*H*), −0.01 (s, 36 H, Si*Me*$_2$) ppm. Anal. Calcd for $C_{20}H_{58}N_3O_2Si_6Yb$ (714.27 g mol^{-1}): C 33.63; H 8.19; N 5.88. Found: C 33.19; H 8.37; N 5.81.

$Sc(OCH_2tBu)_3(AlMe_3)_3$ (3a). To a solution of $[Sc(OCH_2tBu)_3]_4$ (65 mg, 0.20 mmol) in hexane was slowly added a hexane solution of >12 equiv of $AlMe_3$ (46 mg, 0.64 mmol), and the mixture was stirred overnight at ambient temperature. Then, the solvent and the excess $AlMe_3$ were removed in vacuo. The remaining solid was crystallized from hexane at −35 °C to yield **3a** as colorless crystals (112 mg, 0.21 mmol, >99%). IR (Nujol): 1406 w, 1197 s, 1135 m, 1039 s, 1010 s, 936 m, 898 w, 689 vs, 574 s, 529 m, 486 m, 437 w cm^{-1}. ^1H NMR (400.13 MHz, benzene-d_6): δ 3.85 (d, 6 H, C*H*$_2$), 0.90 (d, 27 H, C*Me*$_3$), −0.37 (s br, 27 H, Al*Me*$_3$) ppm. $^{13}C\{^1H\}$ NMR (100.62 MHz, benzene-d_6): δ 80.6, 33.4, 27.1 ppm. Anal. Calcd for $C_{24}H_{60}Al_3O_3Sc$ (522.63 g mol^{-1}): C 55.15; H 11.57. Found: C 55.87; H 11.48.

$Tm(AlMe_4)_3$ (4b). Following the procedure described previously[10d] $TmCl_3(THF)_{3.5}$ (3.67 g, 6.96 mmol), $LiNMe_2$ (1.06 g, 20.87 mmol), and $AlMe_3$ (4.01 g, 55.6 mmol) yielded **4b** as pale green crystals (1.52 g, 3.54 mmol, 52%). ^1H NMR (500 MHz, benzene-d_6): δ −97 (C*H*$_3$) ppm. ^{13}C NMR (125.77 MHz, benzene-d_6): δ −150 ppm. Anal. Calcd for $C_{12}H_{36}Al_3Tm$ (430.3 g mol^{-1}): C 33.50, H 8.43; Found: C 33.55, H 9.14.

$Yb(AlMe_4)_3$ (4c). $YbCl_3(THF)_3$ (2.500 g, 5.043 mmol) was suspended in 80 mL of THF and cooled to −40 °C. $LiNMe_2$ (772 mg, 15.13 mmol) was dissolved in −40 °C cold THF and added to the cold $YbCl_3(THF)_3$ suspension under vigorous stirring. The mixture was allowed to warm to ambient temperature clearing to a light brownish solution but showed formation of an unidentified precipitate quickly. After stirring for 16 h, the solvent was evaporated in oil pump vacuum. Additional suspending of the remaining solid in 30 mL toluene for 1 h and subsequent evaporation to dryness yielded a light brown powder. Upon addition of 80 mL hexane the suspension was cooled to −40 °C. $AlMe_3$ (3.1 g, 43.01 mmol) was added, and the mixture was allowed to warm to ambient temperature. Any additional heating, e.g., from warm stirring plates, was avoided to prevent rapid loss in yield. The mixture turned bright orange and was stirred for 6 h. Volatiles were evaporated in vacuum (CAUTION: excess of $AlMe_3$ and the byproduct $[Me_2AlNMe_2]_2$ are caught in the cooling trap and react violently with air and water, appropriate quenching must be done!) giving an oily residue, which was suspended in hexane. The soluble product was extracted via centrifugation and subsequent filtration of the solution. The orange solution was reduced in volume and cooled to −40 °C for crystallization to yield

Table 6. Crystal Data and Data Collection Parameters of Complexes 2b, 3a, 3b, 4a, 4b, 4c^{LT}, 4c^{HT}, 4c′, and 5b

	2b	3a	3b	4a
chemical formula	$C_{20}H_{58}N_3O_2Si_6Yb$	$C_{24}H_{60}Al_3O_3Sc$	$C_{24}H_{60}Al_3O_3Nd$	$C_{12}H_{36}Al_3Ce$
M_r	714.27	522.63	621.90	401.47
crystal system	monoclinic	hexagonal	hexagonal	monoclinic
space group	$P2_1/c$	$P31c$	$P31c$	$P2_1/c$
a/Å	13.0353(9)	15.8846(3)	16.1210(4)	17.8247(13)
b/Å	16.0013(7)	15.8846(3)	16.1210(4)	18.2909(12)
c/Å	16.8519(11)	8.6025(4)	8.6164(5)	13.7888(10)
α/deg	90.00	90	90	90
β/deg	92.304(5)	90	90	108.531(6)
γ/deg	90.00	120	120	90
V/Å^3	3512.2(4)	1879.78(10)	1939.28(13)	4262.5(5)
Z	4	2	2	8
F(000)	1476	576	654	1640
T/K	173(2)	123(2)	123(2)	100
ρ_{calcd}/g cm^{-3}	1.351	0.923[b]	1.065	1.251
μ/mm^{-1}	2.887	0.283[b]	1.423	1.190
R_1 (obsd)[a]	0.0612	0.0296	0.0153	0.0472
wR_2 (all)[a]	0.0906	0.0886	0.0419	0.0952
GOF (obsd)	1.228	1.110	1.137	1.064

	4b	4c^{LT}	4c^{HT}	4c′	5b
chemical formula	$C_{12}H_{36}Al_3Tm$	$C_{12}H_{36}Al_3Yb$	$C_{12}H_{36}Al_3Yb$	$C_{15}H_{45}Al_4Yb$	$C_{32}H_{80}Al_4Eu_2$
M_r	430.28	434.39	434.39	506.47	876.80
crystal system	monoclinic	monoclinic	monoclinic	monoclinic	trigonal
space group	$C2/c$	$C2/c$	$P2_1/c$	$P2_1/n$	$P3_2$
a/Å	10.8897(13)	10.8877(4)	7.3860(13)	7.4556(9)	11.8535(6)
b/Å	15.7289(19)	15.7129(5)	17.683(6)	20.036(2)	11.8535(6)
c/Å	12.505(2)	12.4928(5)	32.230(11)	17.650(2)	27.0516(14)
α/deg	90	90	90	90	90
β/deg	102.124(2)	101.819(3)	92.52(2)	96.598(9)	90
γ/deg	90	90	90	90	120
V/Å^3	2094.1(5)	2091.92(13)	4205(2)	2619.0(5)	3291.7(3)
Z	4	4	8	4	3
F(000)	864	868	1736	1028	1350
T/K	123(2)	173(2)	213(2)	173(2)	123(2)
ρ_{calcd}/g cm^{-3}	1.365	1.379	1.372	1.284	1.327
μ/mm^{-1}	4.345	4.579	4.556	3.699	2.929
R_1 (obsd)[a]	0.0108	0.0202	0.0626	0.0729	0.0575
wR_2 (all)[a]	0.0275	0.0475	0.1826	0.1184	0.1439
GOF (obsd)	1.116	1.201	1.029	1.270	1.159

[a] $R_1 = \Sigma(||F_o| - |F_c||)/\Sigma|F_o|$; w$R_2 = \{\Sigma[w(F_o^2 - F_c^2)^2]/\Sigma[w(F_o^2)^2]\}^{1/2}$; GOF $= \{\Sigma[w(F_o^2 - F_c^2)^2]/(n-p)\}^{1/2}$. [b] Three disordered hexane molecules not included in density and linear absorption coefficient calculations.

503 mg (0.99 mmol, 20%) $Yb(AlMe_4)_3(Al_2Me_6)_{0.5}$ (**4c′**) as orange crystals. When **4c′** was exposed to vacuum, it lost $AlMe_3$ incorporated into the crystal lattice. Subsequent crystallization from small amounts of hexane yielded 269 mg (0.62 mmol, 12%) of orange crystals of $Yb(AlMe_4)_3$ (**4c**). ^{1}H NMR (500 MHz, toluene-d_8, 25 °C): δ −24 (v br s, CH_3) ppm. IR (Nujol): 1304 m, 1220 vs, 1199 vs, 695 vs, 571 vs, 548 vs, 454 s cm^{-1}. Anal. Calcd for $C_{12}H_{36}Al_3Yb$ (434.403 g mol^{-1}): C 33.18, H 8.35. Found: C 32.86, H 7.98.

[Eu(AlMe$_4$)$_2$]$_n$ (5a). An excess of $AlMe_3$ (160 μL, 1.67 mmol) was added via a micropipet to a yellow solution of $Eu[N(SiHMe_2)_2]_3(THF)_2$ (**2a**, 139 mg, 0.20 mmol) in hexane. Instantaneously, the reaction mixture turned into a suspension and changed colors, first to brownish red, then getting paler and paler toward yellow green. After having stirred for a couple of minutes, the color was gone. The reaction mixture was stirred at ambient temperature for 15 min before a white solid was collected via centrifugation, washed with hexane, and dried under reduced pressure to yield **5a** as a white powder (60 mg, 0.18 mmol, 91%). IR (Nujol): 1197 w, 1171 w, 1072 m, 1026 m, 793 m, 705 s, 633 w, 591 m, 581 m, 560 m cm^{-1}. Anal. Calcd for $C_8H_{24}Al_2Eu$ (326.21 g mol^{-1}): C 29.46, H 7.42; Found: C 29.34, H 7.47.

[Eu(AlEt$_4$)$_2$]$_n$ (5b). An excess of $AlEt_3$ (210 μL, 1.54 mmol) was added via a micropipet to a yellow solution of $Eu[N(SiHMe_2)_2]_3(THF)_2$ (**2a**, 129 mg, 0.19 mmol) in hexane. Instantaneously, the reaction mixture changed colors, first to orange-red, then getting paler and paler to

dx.doi.org/10.1021/ja2001049 |J. Am. Chem. Soc. 2011, 133, 6323–6337

yield a yellow green solution. After stirring for 1 h at ambient temperature the reaction mixture was dried under reduced pressure. The remaining solid was crystallized from hexane at −35 °C to yield **5b** as yellow green crystals (55 mg, 0.13 mmol, 67%). ^{1}H NMR (500 MHz, benzene-d_6): δ 0.16 (br s, $\Delta\nu_{1/2} \approx 44$ Hz, CH_3), −5.62 (v br s, $\Delta\nu_{1/2} \approx 1500$ Hz, CH_2) ppm. ^{13}C NMR (125.77 MHz, benzene-d_6): δ −45.6 (CH_3), −208.9 (CH_2) ppm. Anal. Calcd for $C_{16}H_{40}Al_2Eu$ (438.42 g mol^{-1}): C 43.83, H 9.20. Found: C 41.36, H 9.82.

X-ray Crystallography and Crystal Structure Determination of Complexes 2b, 3a, 3b, 4a, 4b, 4c^{LT}, 4c^{HT}, 4c′, and 5b. Crystals were grown by standard techniques from saturated solutions using hexane at −35 °C. Suitable crystals for diffraction experiments were selected in a glovebox and mounted in Paratone-N (Hampton Research) inside a nylon loop. Data collection was done on STOE IPDS (**2b**, **4a**, **4c^{LT}**, and **4c′**), Enraf Nonius CAD-4 (**4c^{HT}**), Bruker AXS SMART 2K CCD (**3a**, **3b**, and **4b**), and Bruker TXS Apex-II Ultra CCD (**5b**) diffractometers, all except **4a** (Ag radiation, (λ = 0.56085 Å), using graphite monochromated Mo Kα radiation (λ = 0.71073 Å). Final model refinement was done using SHELXL-97.[77a] All plots were generated using the program ORTEP-3.[77b] Further details of the refinement and crystallographic data are listed in Table 6, and in CIF files; CCDC reference numbers 801549−801557.

Computational Details. The complete computational details are given in the Supporting Information. All geometry optimizations were performed using Becke's three-parameter hybrid density functional (B3LYP)[66] in combination with basis sets of valence double-ζ plus polarization quality. The inner electrons of all elements except hydrogen were replaced by relativistic effective core potentials (ECPs).

The total energy and the electronic properties were re-evaluated in single-point (SP) calculations at the optimized geometry using the B3LYP,[66] BPW91,[65] and M06[67] density functionals. Solvent effects for heptane[68] were estimated using an implicit solvent model, the polarizable continuum model (PCM).[78] The PCM calculations were performed using the B3LYP functional and the thus obtained solvent corrections were added also to the BPW91 and M06 energies. The basis sets used in the SP energy calculations were improved compared to those of the geometry optimizations. Whereas the ECPs of the geometry optimizations were retained, the basis sets essentially were of valence triple-ζ quality, extended by polarization and diffuse functions.

In the multivariate regression and data analyses geometrical and electronic molecular descriptors were obtained or extracted from properties obtained using the B3LYP functional. Atomic charges, Wiberg bond indices, and steric exchange energies were calculated using natural bond orbital analysis[60] and natural steric analysis.[79] Unless otherwise noticed, the Allred−Rochow electronegativities,[80] the only common electronegativity scale that is complete for the f-block, and the effective ionic radii (Å) for hexacoordinate metal(III) cations[71] were used as atomic descriptors, number 4 and 25, respectively, in Table S3 in the Supporting Information.

■ ASSOCIATED CONTENT

Supporting Information. CIF files giving full crystallographic data for complexes of **2b**, **3a**, **3b**, **4a**, **4b**, **4c^{LT}**, **4c^{HT}**, **4c′**, and **5b**, ellipsoid plots and selected bond distances and angles of **2b**, **4c^{LT}**, **4c^{HT}**, and **5b** (Figures S1−S4); a variable temperature ^{1}H NMR study of **4c** (Figure S5); thermal degradation ^{1}H NMR studies of **4c** in toluene-d_8 (Figure S6) and cyclohexane-d_{12} (Figure S7); DRIFT spectra of **4c** and $[Yb(AlMe_4)_2]_n$ (Figure S8); complete computational details, calculated energies and Cartesian coordinates of the optimized structures, list of all the molecular descriptors, the numerical values of descriptors, and additional results from and information about the PCA, the cluster analysis, and the multivariate modeling. This material is available free of charge via the Internet at http://pubs.acs.org.

■ AUTHOR INFORMATION

Corresponding Author
vidar.jensen@kj.uib.no; reiner.anwander@uni-tuebingen.de

■ ACKNOWLEDGMENT

The Norwegian Research Council (grants no. 171245/V30 and 177322/V30), L. Meltzers Høyskolefond, the Fonds der Chemischen Industrie, and the Nanoscience program of the University of Bergen are gratefully acknowledged for financial support. The Norwegian Research Council is also acknowledged for CPU resources granted through the NOTUR supercomputing program. We would also like to thank Prof. Wolfgang Scherer and Sandra Altmannshofer for obtaining crystallographic data for complex **4a**.

■ REFERENCES

(1) For reviews, see: (a) Thompson, M. E.; Bercaw, J. E. *J. Pure Appl. Chem.* **1984**, *56*, 1. (b) Watson, P. L.; Parshall, G. W. *Acc. Chem. Res.* **1985**, *18*, 51. (c) Brintzinger, H. H.; Fischer, D.; Mühlhaupt, R.; Rieger, B.; Waymouth, R. M. *Angew. Chem., Int. Ed. Engl.* **1995**, *34*, 1143. (d) *Ziegler Catalysts*; Fink, G., Mühlhaupt, R., Brintzinger, H.-H., Eds.; Springer-Verlag: Berlin, 1995. (e) McKnight, A. L.; Waymouth, R. M. *Chem. Rev.* **1998**, *98*, 2587. (f) Alt, H. G.; Köppl, A. *Chem. Rev.* **2000**, *100*, 1205. (g) Hou, Z.; Wakatsuki, Y. *Coord. Chem. Rev.* **2002**, *231*, 1. (h) Gromada, J.; Carpentier, J. F.; Mortreux, A. *Coord. Chem. Rev.* **2004**, *248*, 397. (i) Bochmann, M. *J. Organomet. Chem.* **2004**, *689*, 3982.

(2) (a) Kaminsky, W.; Kopf, J.; Thirase, G. *Liebigs Ann. Chem.* **1974**, 1531. (b) Kaminsky, W.; Sinn, H. *Liebigs Ann. Chem.* **1975**, 424. (c) Kaminsky, W.; Kopf, J.; Sinn, H.; Vollmer, H. J. *Angew. Chem., Int. Ed. Engl.* **1976**, *15*, 629. (d) Kopf, J.; Kaminsky, W.; Vollmer, H. J. *Cryst. Struct. Commun.* **1980**, *9*, 197. (e) Tebbe, F. N.; Parshall, G. W.; Reddy, G. S. *J. Am. Chem. Soc.* **1978**, *100*, 3611. (f) Howard, T. R.; Lee, J. B.; Grubbs, R. H. *J. Am. Chem. Soc.* **1980**, *102*, 6878. (g) Kopf, J.; Vollmer, H. J.; Kaminsky, W. *Cryst. Struct. Commun.* **1980**, *9*, 271. (h) Kopf, J.; Vollmer, H. J.; Kaminsky, W. *Cryst. Struct. Commun.* **1980**, *9*, 985. (i) Kaminsky, W.; Steiger, R. *Polyhedron* **1988**, *7*, 2375. (j) Siedle, A. R.; Newmark, R. A.; Schroepfer, J. N.; Lyon, P. A. *Organometallics* **1991**, *10*, 400. (k) Guérin, F.; Stephan, D. *Angew. Chem., Int. Ed.* **1999**, *38*, 3698. (l) Kickham, J. E.; Guérin, F.; Stewart, J. C.; Stephan, D. *Angew. Chem., Int. Ed.* **2000**, *39*, 3263. (m) Kickham, J. E.; Guérin, F.; Stewart, J. C.; Urbanska, E.; Stephan, D. *Organometallics* **2001**, *20*, 1175. (n) Yue, N.; Hollink, E.; Guérin, F.; Stephan, D. *Organometallics* **2001**, *20*, 4424. (o) Kickham, J. E.; Guérin, F.; Stephan, D. *J. Am. Chem. Soc.* **2002**, *124*, 11486. (p) Stephan, D. *Organometallics* **2005**, *24*, 2548.

(3) For spectroscopically proposed heteroleptic group 4 tetraalkylaluminate species, see: (a) Bochmann, M.; Lancaster, S. J. *Angew. Chem., Int. Ed. Engl.* **1994**, *33*, 1634. (b) Bochmann, M.; Lancaster, S. J. *J. Organomet. Chem.* **1995**, *497*, 55. (c) Bochmann, M.; Lancaster, S. J. *J. Chem. Soc., Chem. Commun.* **1995**, 2081. (d) Britovsek, P.; Cohen, S. A.; Gibson, V. C.; van Meurs, M. *J. Am. Chem. Soc.* **2004**, *126*, 10701. (e) Petros, R. A.; Norton, J. R. *Organometallics* **2004**, *23*, 5105. (f) Lyakin, O. Y.; Bryliakov, K. P.; Semikolenova, N. M.; Lebedev, A. Y.; Voskoboynikov, A. Z.; Zakharov, V. A.; Talsi, E. P. *Organometallics* **2007**, *26*, 1536. (g) Babushkin, D. E.; Brintzinger, H. H. *Chem.—Eur. J.* **2007**, *13*, 5294.

(4) For spectroscopically proposed heteroleptic iron tetraalkylaluminate species, see: (a) Talsi, E. P.; Babushkin, D. E.; Semikolenova, N. V.; Zudin, V. N.; Panchenko, V. N.; Zakharov, V. A. *Macromol. Chem. Phys.* **2001**, *202*, 2046. (b) Semikolenova, N. V.; Zakharov, V. A.; Talsi, E. P.; Babushkin, D. E.; Sobolev, A. P.; Echevskay, L. G.; Khysniyarov, M. M. *J. Mol. Catal., A: Chem.* **2002**, *182−183*, 283. (c) Zakharov, I. I.; Zakharov, V. A. *Macromol. Theory Simul.* **2004**, *13*, 583.

(5) Bolton, P. D.; Clot, E.; Cowley, A. R.; Mountford, P. *Chem. Commun.* **2005**, 3313.
(6) (a) Hurd, D. T. *J. Org. Chem.* **1948**, *13*, 711. (b) Baker, E. B.; Sisler, H. H. *J. Am. Chem. Soc.* **1953**, *75*, 5193. (c) Gerteis, R. L.; Dickerson, R. E.; Brown, T. L. *Inorg. Chem.* **1964**, *3*, 872.
(7) For reviews, see: (a) Schade, C.; Schleyer, P. v. R. *Adv. Organomet. Chem.* **1987**, *27*, 169. (b) Weiss, E. *Angew. Chem., Int. Ed. Engl.* **1993**, *32*, 1501.
(8) (a) Ziegler, K.; Holzkamp, E. *Liebigs Ann. Chem.* **1957**, *605*, 93. (b) Lehmkuhl, H.; Eisenbach, W. *Liebigs Ann. Chem.* **1967**, *705*, 42. (c) Atwood, J. L.; Stucky, G. D. *J. Am. Chem. Soc.* **1969**, *91*, 2538. (d) Michel, O.; Meermann, C.; Törnroos, K. W.; Anwander, R. *Organometallics* **2009**, *28*, 4783.
(9) (a) Fischbach, A.; Anwander, R. *Adv. Polym. Sci.* **2006**, *204*, 155. (b) Zimmermann, M.; Anwander, R. *Chem. Rev.* **2010**, *110*, 6194.
(10) For homoleptic Ln^{3+} tetraalkylaluminates, see: (a) Evans, W. J.; Anwander, R.; Ziller, J. W. *Organometallics* **1995**, *14*, 1107. (b) Klooster, W. T.; Lu, R. S.; Anwander, R.; Evans, W. J.; Koetzle, T. F.; Bau, R. *Angew. Chem., Int. Ed.* **1998**, *37*, 1268. (c) Fischbach, A.; Klimpel, M. G.; Widenmeyer, M.; Herdtweck, E.; Scherer, W.; Anwander, R. *Angew. Chem., Int. Ed.* **2004**, *43*, 2234. (d) Zimmermann, M.; Frøystein, N. Å.; Fischbach., A.; Sirsch, P.; Dietrich, H. M.; Törnroos, K. W.; Herdtweck, E.; Anwander, R. *Chem.—Eur. J.* **2007**, *13*, 8784.
(11) For homoleptic Ln^{2+} tetraalkylaluminates, see: (a) Klimpel, M. G.; Anwander, R.; Tafipolsky, M.; Scherer, W. *Organometallics* **2001**, *20*, 3983. (b) Sommerfeldt, H.-M.; Meermann, C.; Schrems, M. G.; Törnroos, K. W.; Frøystein, N. A.; Miller, R. J.; Scheidt, E.-W.; Scherer, W.; Anwander, R. *Dalton Trans.* **2008**, 1899.
(12) Anwander, R.; Klimpel, M. G.; Dietrich, H. M.; Shorokhov, D. J.; Scherer, W. *Chem. Commun.* **2003**, 1008.
(13) η^0 (ion separated) coordination mode: (a) Nakamura, H.; Nakayama, Y.; Yasuda, H.; Maruo, T.; Kanehisa, N.; Kai, Y. *Organometallics* **2000**, *19*, 5392. (b) Arndt, S.; Spaniol, T. P.; Okuda, J. *Angew. Chem., Int. Ed.* **2003**, *42*, 5075.
(14) η^1 coordination mode: (a) Zimmermann, M.; Törnroos, K. W.; Anwander, R. *Angew. Chem., Int. Ed.* **2007**, *46*, 3126. (b) Litlabø, R.; Zimmermann, M.; Saliu, K.; Takats, J.; Törnroos, K. W.; Anwander, R. *Angew. Chem., Int. Ed.* **2007**, *46*, 3126.
(15) η^2 is considered the routine coordination mode, which was originally detected in $(C_5H_5)_2Ln(AlMe_4)$ (Ln = Y, Yb): (a) Holton, J.; Lappert, M. F.; Scollary, G. R.; Ballard, D. G. H.; Pearce, R.; Atwood, J. L.; Hunter, W. E. *J. Chem. Soc., Chem. Comm.* **1976**, 425. (b) Scollary, G. R. *Aust. J. Chem.* **1978**, *31*, 41.
(16) η^3 coordination mode: (a) Dietrich, H. M.; Schuster, O.; Törnroos, K. W.; Anwander, R. *Angew. Chem., Int. Ed.* **2006**, *45*, 4858. (b) Reference 12. (c) R. Litlabø, R.; Lee, H. S.; Niemeyer, M.; Törnroos, K. W.; Anwander, R. *Dalton Trans.* **2010**, *39*, 6815.
(17) μ-η^1:η^1 coordination mode: (a) Evans, W. J.; Chamberlain, L. R.; Ulibarri, T. A.; Ziller, J. W. *J. Am. Chem. Soc.* **1988**, *110*, 6423. (b) Dietrich, H. M.; Törnroos, K. W.; Herdtweck, E.; Anwander, R. *Organometallics* **2009**, *28*, 6739 and references therein.
(18) μ-η^1:η^2 coordination mode: (a) Reference 14. (b) Zimmermann, M.; Volbeda, J.; Törnroos, K. W.; Anwander, R. *C. R. Chim.* **2010**, *13*, 651.
(19) μ-η^1:η^3 coordination mode: see refs 9 and 11.
(20) For recent examples, see: (a) Zimmermann, M.; Törnroos, K. W.; Sitzmann, H.; Anwander, R. *Chem.—Eur. J.* **2008**, *14*, 7266. (b) Sommerfeldt, H.-M.; Meermann, C.; Törnroos, K. W.; Anwander, R. *Inorg. Chem.* **2008**, *47*, 4696. (c) Korobkov, I.; Gambarotta, S. *Organometallics* **2009**, *28*, 4009. (d) Korobkov, I.; Gambarotta, S. *Organometallics* **2009**, *28*, 5560.
(21) For recent examples, see: (a) Le Roux, E.; Nief, F.; Jaroschik, F.; Törnroos, K. W.; Anwander, R. *Dalton Trans.* **2007**, 4866. (b) Litlabø, R.; Saliu, K.; Ferguson, M. J.; McDonald, R.; Takats, J.; Anwander, R. *Organometallics* **2009**, *28*, 6750.
(22) For examples, see: (a) Fischbach, A.; Perdih, F.; Herdtweck, E.; Anwander, R. *Organometallics* **2006**, *25*, 1626. (b) Zhang, L.; Nishiura, M.; Yuki, M.; Hou, Z. *Angew. Chem., Int. Ed.* **2008**, *47*, 2642. (c) Liu, B.; Liu, X.; Cui, D.; Liu, L. *Organometallics* **2009**, *28*, 1453.
(23) (a) Evans, W. J.; Ansari, M. A.; Ziller, J. W.; Khan, S. I. *Inorg. Chem.* **1996**, *35*, 5435. (b) Gordon, J. C.; Giesbrecht, G. R.; Clark, D. L.; Hay, P. J.; Keogh, D. W.; Poli, R.; Scott, B. L.; Watkin, J. G. *Organometallics* **2002**, *21*, 4726. (c) Giesbrecht, G. R.; Gordon, J. C. *Dalton Trans.* **2004**, 2387. (d) Scott, J.; Basuli, F.; Fout, A. R.; Huffman, J. C.; Mindiola, D. J. *Angew. Chem., Int. Ed.* **2008**, *47*, 8502.
(24) (a) Dietrich, H. M.; Törnroos, K. W.; Anwander, R. *J. Am. Chem. Soc.* **2006**, *128*, 9298. (b) Litlabø, R.; Zimmermann, M.; Saliu, K.; Takats, J.; Törnroos, K. W.; Anwander, R. *Angew. Chem., Int. Ed.* **2008**, *47*, 9560. (c) Scott, J.; Fan, H.; Wicker, B. F.; Fout, A. R.; Baik, M.-H.; Mindiola, D. J. *J. Am. Chem. Soc.* **2008**, *130*, 14438.
(25) Dietrich, H. M.; Grove, H.; Törnroos, K. W.; Anwander, R. *J. Am. Chem. Soc.* **2006**, *128*, 1458.
(26) (a) Gerber, L. C. H.; Le Roux, E.; Törnroos, K. W.; Anwander, R. *Chem.—Eur. J.* **2008**, *14*, 9555. (b) Venugopal, A.; Kamps, I.; Bojer, D.; Berger, R. J. F.; Mix, A.; Willner, A.; Neumann, B.; Stammler, H.-G.; Mitzel, N. W. *Dalton Trans.* **2009**, 5755.
(27) For reviews, see: (a) Giesbrecht, G. R.; Gordon, J. C. *Dalton Trans.* **2004**, 2387. (b) Scott, J.; Mindiola, D. J. *Dalton Trans.* **2009**, 8463.
(28) Parts of this work were already communicated: (a) Meermann, C.; Occhipinti, G.; Dietrich, H. M.; Törnroos, K. W.; Jensen, V. R.; Anwander, R. 23rd International Conference on Organometallic Chemistry (ICOMC 2008), July 13−18, 2008, Rennes, France. (b) Anwander, R. 7th International Conference on f Elements (ICfE 7), August 23−27, 2009, Cologne, Germany.
(29) Holton, J.; Lappert, M. F.; Ballard, D. G. H.; Pearce, R.; Atwood, J. L.; Hunter, W. E. *J. Chem. Soc., Dalton Trans.* **1979**, 54.
(30) Estler, F. Ph.D. thesis, Technische Universität München, 2003.
(31) Robert, D.; Spaniol, T. P.; Okuda, J. *Eur. J. Inorg. Chem.* **2008**, 2801.
(32) Carver, C. T.; Monreal, M. J.; Diaconescu, P. L. *Organometallics* **2008**, *27*, 363.
(33) Day, M. W.; Bercaw, J. E.; Zubris, D. L. private communication, 2003, CCDC 103059.
(34) Day, M. W.; Schofer, S. J.; Bercaw, J. E. private communication, 2005, CCDC 192902.
(35) Fischbach, A. Ph.D. thesis, Technische Universität München, 2003.
(36) Dietrich, H. M.; Raudaschl-Sieber, G.; Anwander, R. *Angew. Chem., Int. Ed.* **2005**, *44*, 5303.
(37) Evans, W. J.; Anwander, R.; Doedens, R. J.; Ziller, J. W. *Angew. Chem., Int. Ed.* **1994**, *33*, 1641.
(38) Boyle, T. J.; Ottley, L. A. M.; Daniel-Taylor, S. D.; Tribby, L. J.; Bunge, S. D.; Costello, A. L.; Alam, T. M.; Gordon, J. C.; McCleskey, T. M. *Inorg. Chem.* **2007**, *46*, 3705.
(39) Fischbach, A.; Meermann, C.; Eickerling, G.; Scherer, W.; Anwander, R. *Macromolecules* **2006**, *39*, 6811.
(40) Biagini, P.; Lugli, G.; Abis, L.; Millini, R. *J. Organomet. Chem.* **1994**, *474*, C16.
(41) Garbassi, F.; Biagini, P.; Andreussi, P.; Lugli, G. Eur. Pat. Appl. 1995, EP 638598 A1 19950215.
(42) Evans, W. J.; Boyle, T. J.; Ziller, J. W. *J. Am. Chem. Soc.* **1993**, *115*, 5084.
(43) Shan, C.-J.; Lin, Y.-H.; Jin, S.-C.; Jun, O.; Fan, Y.-G.; Yang, G.-D.; Yu, J.-S. *Acta Chim. Sin.* **1987**, *45*, 949.
(44) Evans, W. J.; Boyle, T. J.; Ziller, J. W. *J. Organomet. Chem.* **1993**, *462*, 141.
(45) Fischbach, A.; Herdtweck, E.; Anwander, R. *Inorg. Chim. Acta* **2006**, *359*, 4855.
(46) Fischbach, A.; Eickerling, G.; Scherer, W.; Herdtweck, E.; Anwander, R. *Z. Naturforsch.* **2004**, *59b*, 1353.
(47) Fischbach, A.; Herdtweck, E.; Anwander, R.; Eickerling, G.; Scherer, W. *Organometallics* **2003**, *22*, 499.
(48) Giesbrecht, G. R.; Gordon, J. C.; Brady, J. T.; Clark, D. L.; Keogh, D. W.; Michalczyk, R.; Scott, B. L.; Watkin, J. G. *Eur. J. Inorg. Chem.* **2002**, *2002*, 723.
(49) Gordon, J. C.; Giesbrecht, G. R.; Brady, J. T.; Clark, D. L.; Keogh, D. W.; Scott, B. L.; Watkin, J. G. *Organometallics* **2002**, *21*, 127.

(50) Evans, W. J.; Ansari, M. A.; Ziller, J. W. *Inorg. Chem.* **1995**, *34*, 3079.
(51) Bradley, D. C.; Ghotra, J. S.; Hart, F. A. *J. Chem. Soc., Dalton Trans.* **1973**, 1021.
(52) (a) Andersen, R. A.; Templeton, D. H.; Zalkin, A. *Inorg. Chem.* **1978**, *17*, 2317.(b) The similar unit cell parameters of $Nd[N(SiMe_3)_2]_3$ (*a*, *b* = 16.476(13) Å, *c* = 8.485(7) Å)[52a] and **3b** (*a*, *b* = 16.1210(4) Å, *c* = 8.6164(5) Å) caused some confusion during the X-ray structure analysis.
(53) For a topological analysis of the total electron density of $Y(AlR_4)_3$ (R = Me, Et) using Baders "Atoms in Molecules" (AIM) approach and DFT calculations on $Y(AlR_4)_3$ (R = Me, Et), see ref 11a.
(54) For DFT studies of rare earth metal alkyl complexes, see: (a) Clark, D. L.; Gordon, J. C.; Hay, P. J.; Martin, R. L.; Poli, R. *Organometallics* **2002**, *21*, 5000. (b) Perrin, L.; Maron, L.; Eisenstein, O.; Lappert, M. F. *New J. Chem.* **2003**, *27*, 121.
(55) For DFT studies of cationic group 4 AlR_3 (Me, *i*Bu) adduct complexes, see: (a) Vanka, K.; Chan, M. S. W.; Pye, C. C.; Ziegler, T. *Organometallics* **2000**, *19*, 1841. (b) Bolton, P. D.; Adams, N.; Clot, E.; Cowley, A. R.; Wilson, P. J.; Schröder, M.; Mountford, P. *Organometallics* **2006**, *25*, 5549.
(56) Malinowski, E. R. *Factor Analysis in Chemistry*, 3 ed.; Wiley: New York, 2002.
(57) Wise, B. M; Gallagher, N. B.; Bro, R.; Shaver, J. M.; Windig, W.; Koch, R. S. PLS_Toolbox version 3.5 manual; Eigenvector Research: Manson, WA, 2004.
(58) (a) Jackson, J. E.; Mudholkar, G. S. *Technometrics* **1979**, *21*, 341. (b) Winer, B. J.; Brown, D. R.; Michels, K. M. *Statistical Principles in Experimental Design*, 3rd ed.; McGraw-Hill: New York, 1991. (c) Reference 57.
(59) Mahalanobis, P. C. *Proc. Natl. Inst. Sci. India* **1936**, *2*, 49.
(60) (a) Reed, A. E.; Weinstock, R. B.; Weinhold, F. *J. Chem. Phys.* **1985**, *83*, 735.(b) Glendening, E. D.; Badenhoop, J. K.; Reed, A. E.; Carpenter, J. E.; Bohmann, J. A.; Morales, C. M.; Weinhold, F. *NBO 5.0*; Theoretical Chemistry Institute: University of Wisconsin, Madison, 2001.
(61) The percentage of the aluminium character in the three-center two-electron (M−C−Al) natural bond is typically 12−15%.
(62) Visscher, L.; Dyall, K. G. *At. Data Nucl. Data Tables* **1997**, *67*, 207.
(63) Marks, T. J. *Science* **1982**, *217*, 989.
(64) (a) Blomberg, M. R. A.; Siegbahn, P. E. M.; Nagashima, U.; Wennerberg, J. *J. Am. Chem. Soc.* **1991**, *113*, 424. (b) Deubel, D. V.; Ziegler, T. *Organometallics* **2002**, *21*, 1603. (c) Frenking, G.; Fröhlich, N. *Chem. Rev.* **2000**, *100*, 717. (d) Sparta, M.; Børve, K. J.; Jensen, V. R. *J. Phys. Chem. A* **2006**, *110*, 11711.
(65) (a) Becke, A. D. *Phys. Rev. A* **1988**, *38*, 3098. (b) Perdew, J. P.; Wang, Y. *Phys. Rev. B* **1992**, *45*, 13244.
(66) Becke, A. D. *J. Chem. Phys.* **1993**, *98*, 5648.
(67) Zhao, Y.; Truhlar, D. G. *Acc. Chem. Res.* **2008**, *41*, 157.
(68) The solvent used in the experiments was *n*-hexane. This solvent is not defined in Gaussian 03, and thus heptane was used instead in the calculations. These two solvents have similar properties. For example, the dielectric constants of heptane and *n*-hexane are 1.92 and 1.88, respectively.
(69) Titanium and thorium were detected as unusual samples because they both had high leverage as well as high studentized residual (poor fit to the corresponding *y*-values) in the model. Despite the fact that actinium and lanthanum were detected as unusual samples in the PCA, the analysis of the plot leverage vs studentized residual shows that they are not unusual samples in the PLS model.
(70) The negative influence of metal electronegativity on the ligand stability is demonstrated by the positive correlation that this descriptor displays with the "sum of the natural charge on all Al atoms", $R^2 = 0.48$, and the negative correlation with the Wiberg bond index, total by atom (sum over all Al atoms), $R^2 = 0.49$. These two descriptors, not included in the final multivariate model, show that when the metal electronegativity increases, the charge on the aluminum atoms increases. At the same time the $Al-CH_3$ bonds become weaker.
(71) Shannon, R. D. *Acta Crystallogr. A* **1976**, *32*, 751.
(72) (a) Reinheckel, H. *Angew. Chem.* **1963**, *75*, 1206. (b) Dietrich, H. M.; Ziller, J. W.; Anwander, R.; Evans, W. J. *Organometallics* **2009**, *28*, 1173.
(73) Johnson, D. A.; Emeléus, H. J.; Sharpe, A. G. In *Advances in Inorganic Chemistry*; Academic Press: New York, 1977; Vol. 20.
(74) Preferred reduction of $Sm(AlMe_4)_3$ in the presence of sterically demanding ligands has been reported recently: (a) Reference 20a. (b) Bojer, D.; Venugopal, A.; Neumann, B.; Stammler, H.-G; Mitzel, N. W. *Angew. Chem., Int. Ed.* **2010**, *49*, 2448.
(75) Alyea, E. C.; Bradley, D. C.; Copperthwaite, R. G. *J. Chem. Soc., Dalton Trans.* **1972**, 1580.
(76) Anwander, R.; Runte, O.; Eppinger, J.; Gerstberger, G.; Herdtweck, E.; Spiegler, M. *J. Chem. Soc., Dalton Trans.* **1998**, 847.
(77) (a) Sheldrick, G. M. *Acta Crystallogr.* **2008** *A64*, 112. (b) Burnett, M. N.; Johnson, C. K. *ORTEP-III: Oak Ridge Thermal Ellipsoid Plot Program for Crystal Structure Illustrations*, ORNL-6895; Oak Ridge National Laboratory: Oak Ridge, TN, 1996.
(78) (a) Tomasi, J.; Persico, M. *Chem. Rev.* **1994**, *94*, 2027. (b) Cossi, M.; Scalmani, G.; Rega, N.; Barone, V. *J. Chem. Phys.* **2002**, *117*, 43.
(79) Badenhoop, J. K.; Weinhold, F. *J. Chem. Phys.* **1997**, *107*, 5422.
(80) Allred, A. L.; Rochow, E. G. *J. Inorg. Nucl. Chem.* **1958**, *5*, 264.